

Stochastic instability of synchronisation of oscillators on networks

Mathew Zuparic^a, Alexander C. Kalloniatis^b

^a*Departamento de Fisica, Universidade Federal de Sao Carlos, Sao Carlos, Brazil*

^b*Defence Science and Technology Organisation, Canberra, ACT 2600, Australia*

Abstract

We consider the effect of correlated noise on the stability of synchronisation of oscillators on a general network. By examining the Kuramoto model in the neighborhood of a global phase synchronised fixed point the impact of the noise is seen in the time-dependent probability density. If the support of the distribution evolves outside the basin of attraction of a fixed point with finite probability the system is deemed to be unstable. By exactly solving the Fokker-Planck equation we find that quite different instabilities follow. For uncorrelated noise the instability is exponentially suppressed: for small diffusion constant, there is a vanishingly small probability that the system can drift out of phase synchronicity. With correlated noise applied to oscillator frequencies and the network coupling, the peak of the probability distribution itself drifts outside the basin of the fixed point and suppression becomes power-law. Correlated noise can therefore strongly de-stabilise phase synchronicity. The significance of result for general networks is discussed.

Keywords: synchronisation oscillator Kuramoto noise Fokker-Planck probability orthogonal polynomials

2010 MSC: 33D50 34F05

1. Introduction

The spontaneous generation of ordered or patterned behaviour is a significant property of nonlinear dynamical systems of many coupled heterogeneous entities. This behaviour is argued to be relevant to a vast array of real

URL: `zuparic@df.ufscar.br` (Alexander C. Kalloniatis),
`alexander.kalloniatis@dsto.defence.gov.au` (Alexander C. Kalloniatis)

world systems: physical, chemical, biological, ecological and social. Where the dynamics of the component level entities have cyclic characteristics, the model of coupled phase oscillators on a network is a compact mathematical representation offering much insight. The Kuramoto model [1] is one especially simple example of this, exhibiting a clear transition from incoherence to phase synchrony as a single coupling constant is varied from small to large positive values. In this paper we explore how different ways of injecting noise - or stochastic fluctuations - from a regime close to the synchronised state can generate instability.

The Kuramoto model [1] involves one-dimensional phase oscillators described by angles θ_i coupled on a network described by an undirected graph G of size N and is given by the first order differential equation,

$$\dot{\theta}_i = \omega_i - \frac{K}{N} \sum_{j=1}^N A_{ij} \sin(\theta_i - \theta_j), \quad 1 \leq i \leq N. \quad (1)$$

Here A_{ij} is the adjacency matrix encoding the graph structure, ω_i are intrinsic frequencies of the oscillators, usually drawn from some statistical distribution, and K is a global coupling controlling the rapidity and strength of mutual adjustment between adjacent oscillators. A good overview of this and related models is given by Strogatz [2]. At zero coupling the system behaves incoherently with each oscillator moving in simple harmonic motion according to its intrinsic frequency. Increasing the coupling drives the population into synchrony, with some of the oscillators locking into a single core that moves with harmonic motion according to the frequency average over the whole oscillator ensemble. Kuramoto [1] originally considered only the complete ($A_{ij} = 1$) infinite ($N \rightarrow \infty$) case, which lends itself to solution via a variety of techniques from fluid dynamics. In this context, stability and noise have been studied using the continuum limit [3, 4]. However, these techniques are difficult to generalise to non-complete finite graphs. Numerical studies, such as [5], have shed light on the path towards synchronisation for different network topologies but it is difficult to draw specific conclusions about stability from these.

A contrasting class of dynamical models of the form

$$\dot{\phi}_i = f(\phi_i) + \sigma \sum_j A_{ij} [g(\phi_j) - g(\phi_i)] \quad (2)$$

have also been tested for stability in the vicinity of fixed points characterising synchrony. Using spectral graph theory, Pecora and Carroll [6] formulated a

Master Stability Equation from Eq.(2) which identified stability as a property of the spectrum of the graph Laplacian (to be defined below) of the underlying network. As usual in the Lyapunov approach, a fixed point ϕ_i^* (associated here with phase synchrony) is perturbed by fluctuations $\phi_i^* + \eta_i$ and inserted into the dynamical equations. By isolating powers of η up to first order (η is ‘small’: $\eta^2 \approx 0$) solutions for both the fixed point and the fluctuations can be obtained. In this respect, the difference between the Kuramoto model Eq.(1) and Eq.(2) lies in the interactions of the former depending on a function of phase differences and the latter a difference of a function of the phases. This seemingly innocuous distinction means that within such first order considerations the phase synchrony of the Kuramoto model is globally stable (one must go to second order in fluctuations to detect instabilities here [7]) while for models of the form Eq.(2) rich instabilities can be identified more straightforwardly.

However, not all properties of real world systems, such as the ‘fine-structure’ of component entities below the length or time scales of human observation, can be systematically encoded in deterministic equations of motion. This is where ‘noise’ or stochastic fluctuations in equations of motion are invoked. The stability in the presence of noise of a key nonlinear system property such as synchrony is therefore important in eventually applying such elementary mathematical models to real world systems. Park and Kim [8, 9] have numerically examined noise in the Kuramoto model but for the limited case of equal frequencies and a complete network (and also using an extra ‘pinning term’). While giving deep insights into new types of meta-stable states for this case, no conclusions can be drawn for inhomogeneous frequency distributions and general graphs (each case of interest has to be separately simulated).

The ability to treat general graphs and frequency distributions is where analytic approaches, such as the Lyapunov approach to deterministic stability, come into their own. However going beyond the Lyapunov approach for the Kuramoto model has its challenges. Fluctuations for the deterministic case correspond to instantaneously shifting the system from a fixed point but then allowing the deterministic system behaviour of Eqs.(1,2) govern the subsequent evolution. Stochastic fluctuations, contrastingly, involve sustained erratic perturbation away from the deterministic trajectories. Mathematically this is not so easily cast into the fluctuation equations like $\dot{\eta} \propto \eta$ of deterministic systems. For the Kuramoto model the nonlinearities are non-polynomial (a cosine rather than, say, quartic potential energies whose turn-

ing points define a boundary across which ‘first passage time’ for diffusion can be computed). A slightly weaker approach solves the Fokker-Planck equation for the time-dependent probability distribution for noise fluctuations in the vicinity of a fixed point. One identifies then whether the stochastic dynamics will keep the system in that vicinity or allow it to escape [10]. Instability of the stochastic system can be thereby detected.

In terms of the Kuramoto model in the vicinity of phase synchrony noise be injected by three basic ways: through the coupling, the frequencies, and the network topology. We consider combinations of the first two methods while treating the underlying network fixed. However, in the neighborhood of phase synchrony the system decouples into independent behaviours of modes corresponding to eigenvectors of the graph Laplacian just as in the approach of Pecora and Carroll [6] to systems like Eq.(2). We therefore apply the noise (to coupling and frequencies) independently for each such mode of the system. When this noise is introduced correlated strong stochastic instabilities are generated, in the sense just discussed. We solve, for a variety of cases, the stationary probability distributions. In some cases we are able to go even further and analytically solve for the time-dependent probability distributions. In considering the application to general networks we are able to deduce that phase synchronisation on networks with many poorly connected subgraphs (such as sparse random graphs and scale-free graphs) is more susceptible to stochastic instability.

The paper is structured as follows. We formulate the model in the next section, and then discuss our solution method for the Fokker-Planck system. To streamline the paper we next state the main results for the probability distribution functions with minimal derivation (the laborious detail is laid out in Appendices at the end of the paper). We then deduce the cases where instability applied. Subsequently we consider some special parameter cases and plot the probability density functions. The paper concludes with a discussion where we draw implications of our results for general graphs, compare our results to known cases in the literature and look ahead to future work. The detail of our derivations is presented in a series of seven appendices.

2. Stochastic equations close to synchrony

2.1. Laplacian decomposition of deterministic case

We wish to consider the system Eq.(1) for a connected graph G close to synchrony. To this end it is useful to use the Laplacian [11] for G ,

$$L_{ij} = d_i \delta_{ij} - A_{ij}, \quad (3)$$

with d_i is the degree of node i . The spectrum of Laplacian eigenvalues λ_i is positive semi-definite, as explained in Appendix A. The corresponding system of orthonormal eigenvectors is given by,

$$\sum_{j=1}^N L_{ij} \nu_j^{(r)} = \lambda_r \nu_i^{(r)}, \quad \sum_{i=1}^N \nu_i^{(r)} \nu_i^{(s)} = \delta_{rs}.$$

Some relevant theorems involving the Laplacian spectrum are summarised in Appendix A. Most immediately useful here is the property that the lowest eigenvalue vanishes, $\lambda_0 = 0$. For a connected graph G the first non-zero eigenvalue λ_1 is positive and known as the algebraic connectivity [12]. The corresponding eigenvector is called the *Fiedler*. Graphs with $\lambda_1 < 1$ are easily disconnected by removal of a small number of links. The eigenvectors $\vec{\nu}^{(r)}$ also have a network interpretation. They represent weighted *sub-graphs* of G : the (not necessarily positive) numerical weight with which a node i is represented in the Laplacian eigenmode r is given by the component $\nu_i^{(r)}$.

The Laplacian is in fact a Laplace-Beltrami operator on the manifold described by G . To this extent it reflects properties well-known in condensed matter systems: the eigenvalues λ_r are a ‘momentum-squared’ and their corresponding eigenvectors act like ‘probes’ on substructures of the graph. The eigenvectors corresponding to low-lying eigenvalues $r \sim 1$ involve larger scale sub-graphs of G while those for higher values $r \sim N$ reflect finer structures in the graph. This will be useful in interpreting our results.

We now expand a phase angle of the Kuramoto model in the Laplacian basis of eigenmodes,

$$\theta_i(t) = \sum_{r=0}^{N-1} x_r(t) \nu_i^{(r)}. \quad (4)$$

Treating ω_i as the components to an N -dimensional vector, $\vec{\omega}$, with $\bar{\omega}$ the average over the frequency distribution, we can form the scalar product of

the frequency vector and the Laplacian eigenvectors

$$\omega^{(r)} = \vec{\omega} \cdot \vec{\nu}^{(r)}.$$

Turning to the Kuramoto model, and combining K/N into a coupling constant σ , we consider the system close to a point of global phase synchronisation ($\theta_i \approx \theta_j \forall i, j$),

$$\begin{aligned} \dot{\theta}_i &\approx \omega_i - \sigma \sum_j A_{ij}(\theta_i - \theta_j) \\ &= \omega_i - \sigma \sum_j L_{ij} \theta_j. \end{aligned} \quad (5)$$

Inserting the expansion Eq.(4) into the truncated equation of motion Eq.(5), we can extract equations for the normal eigenmodes $r \neq 0$,

$$\dot{x}_r(t) = \omega^{(r)} - \sigma \lambda_r x_r(t) \quad (6)$$

while the zero mode of Eq.(5) gives $x_0(t) = \sqrt{N}(t - t')\bar{\omega}$ at time t after initial time t' . To this order, the modes r are decoupled. The exact solution to Eq.(6) is:

$$x_r(t) = x'_r e^{-\sigma \lambda_r (t-t')} + \frac{\omega^{(r)}}{\sigma \lambda_r} \left(1 - e^{-\sigma \lambda_r (t-t')}\right) \quad (7)$$

where $x'_r = x_r(t')$ represents the initial configuration. Taking the large t limit of this shows that there is a fixed point

$$x_r^* = \frac{\omega^{(r)}}{\sigma \lambda_r} \quad (8)$$

whose stability is determined by the exponents $-\sigma \lambda_r$. These are effectively the Lyapunov exponents and they do not change sign due to the semi-definiteness of the Laplacian spectrum (see Appendix A). As discussed by one of us elsewhere [7], this shows that global phase synchrony is stable in every direction of trajectory space (which can be labelled by the modes r): fluctuations on $\theta_i = \theta_j \forall i, j$ are small,

$$|x_r(t)| \ll 1 \quad \forall t \quad (9)$$

as long as the condition is true at the initial time $t = t'$, and

$$|x_r^*| \equiv \left| \frac{\omega^{(r)}}{\sigma \lambda_r} \right| \ll 1 \quad (10)$$

so that the approximations leading to Eq.(5) are valid over all times. The quantity x_r^* defines the origin of a ‘basin of attraction’ in trajectory space whose curvature in every direction of the origin is concave (since the $\sigma \lambda_r$ do not change sign).

This leads to the following simple intuitive picture to which we shall often return. The Laplacian eigenmodes with largest values of $\frac{|\omega^{(r)}|}{\sigma \lambda_r}$ indicate whether the system can phase synchronise or not. This ratio brings together the three key elements of the dynamical system: the frequencies, the network topology (in the eigenvalues and eigenvectors) and the coupling constant. There are a number of ways these may combine to satisfy Eq.(10). Two obvious cases are sufficiently strong coupling and/or sufficiently narrow frequency range. Modes r with large λ_r also satisfy Eq.(10). Easily disconnected graphs have $\lambda_r < 1$ and therefore require larger coupling to globally phase synchronise. This is also intuitively sensible. However - in light of our comments about eigenvectors above - the λ_r for $r \sim 1$ correspond to coarser structures so that there will be more nodes represented in the eigenvector $\nu^{(r)}$ giving possibly larger values of $\omega^{(r)}$. Thus the mode most susceptible to disruption from synchronicity is that for which $\frac{\omega^{(r)}}{\sigma \lambda_r}$ is closest to one. We call this the *critical mode*. Because of the interplay of quantities in the ratio in x_r^* this mode may not be that corresponding to $r = 1$.

We obtain a *weak* type of criterion for synchronisation (see also [13]), $\sigma \gg |\omega^{(r)}|/\lambda_r \forall r$. But because we cannot determine a boundary to the basin we therefore cannot, at this order, extract a sharp threshold of coupling which distinguishes synchrony from incoherence as distinct phases. To detect instability for the deterministic case one must go to second order in fluctuations [7]. Possible instabilities induced by noise, the stochastic case, are our concern in this paper.

2.2. Stochastic system in Laplacian decomposition

The famous logistic equation $\dot{x} = x(1 - x)$ for population dynamics can be brought to the form Eq.(6) after a change of variables. This is our clue for examining this system in the presence of stochastic fluctuations. In terms of phase synchronisation, this relationship is understood by seeing the normal mode fluctuations x_r in terms of population species [7]. The Laplacian

normal modes correspond to a variety of ‘species’. Extinction of a species amounts to approach to the phase synchronised fixed point, namely stability of the fixed point; extinction of all species is equivalent to the system being at the phase synchronised fixed point. Growth corresponds to departure from the phase synchronised fixed point, namely instability of the fixed point. Bringing stochastic fluctuations into the picture now enables us to exploit a significant body of work on noisy population dynamics. Specifically, in [14] and references therein, Gońa considered a generalisation of the logistic equation by perturbation with two correlated Gaussian White Noise (GWN) terms, $\Gamma_r^{(a)}$ and $\Gamma_r^{(m)}$; the superscripts a and m stand for additive and multiplicative respectively. We perform a similar analysis by perturbing Eq.(6) for each eigenmode via the following substitutions,

$$\begin{aligned}\omega^{(r)} &\rightarrow \omega^{(r)} + \gamma_2^{(r)} \Gamma_r^{(a)}(t) \\ \sigma &\rightarrow \sigma + \frac{\gamma_1^{(r)}}{\lambda_r} \Gamma_r^{(m)}(t)\end{aligned}\tag{11}$$

where $\{\gamma_1^{(r)}, \gamma_2^{(r)}\} \in \mathbb{R}$. The resulting Langevin equations are

$$\dot{x}_r(t) = \left(\omega^{(r)} + \gamma_2^{(r)} \Gamma_r^{(a)}(t) \right) - \left(\sigma \lambda_r + \gamma_1^{(r)} \Gamma_r^{(m)}(t) \right) x_r(t)\tag{12}$$

We see the meaning now of the terms ‘additive’ and ‘multiplicative’ in terms of how they manifest noise into the equation of motion: the former introduce a time dependent randomness on the intrinsic frequencies, $\omega^{(r)}$, and the latter term introduces it on the coupling, σ . We emphasise that the fluctuations Eq.(11) are introduced for each Laplacian eigenmode, leading to a localisation of the effective coupling.

In light of this, we adopt an approach which probes specifically the sensitivity of the aforementioned critical modes to noise by targeting stochastic fluctuations to specific clusters of the network. The clusters are determined by the Laplacian eigenmode decomposition.

The additive and multiplicatively GWN terms are themselves given in terms of uncorrelated GWN functions $\Gamma_r^{(1)}$ and $\Gamma_r^{(2)}$ through

$$\Gamma_r^{(a)}(t) = c_r \Gamma_r^{(1)}(t) + \sqrt{|1 - c_r^2|} \Gamma_r^{(2)}(t), \quad \Gamma_r^{(m)} = \Gamma_r^{(1)}, \quad c_r \in \mathbb{R},\tag{13}$$

where the following expectation values encode the absence of correlation between $\Gamma_r^{(1)}$ and $\Gamma_r^{(2)}$:

$$\langle \Gamma_r^{(1)}(t) \rangle = \langle \Gamma_r^{(2)}(t) \rangle = \langle \Gamma_r^{(1)}(t) \Gamma_r^{(2)}(t') \rangle = 0$$

$$\langle \Gamma_{r_1}^{(1)}(t) \Gamma_{r_2}^{(1)}(t') \rangle = \langle \Gamma_{r_1}^{(2)}(t) \Gamma_{r_2}^{(2)}(t') \rangle = \Omega \delta_{r_1 r_2} \delta(t - t').$$

The quantity Ω is the diffusion constant. As Ω approaches zero we expect to obtain the usual deterministic results. Hence $\Gamma_r^{(a)}$ and $\Gamma_r^{(m)}$ are correlated in the following way,

$$\langle \Gamma_{r_1}^{(a)}(t) \Gamma_{r_2}^{(m)}(t') \rangle = c_{r_1} \Omega \delta_{r_1 r_2} \delta(t - t') , \quad \Omega \in \mathbb{R} \quad (14)$$

We refer to the constant c_r as the *correlation parameter*. For more detail on Langevin equations and GWN the reader is referred to Chap. 3 of [15].

Rather than focusing on x_r in the Langevin equations (or specifically, associated ‘random variables’ X_r) we shall address the corresponding probability density function associated. Denoted P , it determines the probability that the system lies in a state $x_r \leq X_r \leq x_r + dx_r$. The Fokker-Planck equation governs the evolution of this probability density, given the system is initially in state $X_r = x'_r$ at initial time t' :

$$\begin{aligned} P(\vec{x}, t) &\equiv P(\vec{x}, \vec{x}' | t, t') \\ P(\vec{x}, t') &= \delta(\vec{x} - \vec{x}') \end{aligned}$$

where \vec{x} now represents the vector of components x_r . From the Langevin equation Eq.(12) we obtain, using [15], the following Fokker Planck equation,

$$\frac{\partial}{\partial t} P(\vec{x}, t) = \sum_{r=1}^{N-1} \frac{\partial^2}{\partial x_r^2} \{ s^{(r)}(x_r) P(\vec{x}, t) \} - \sum_{r=1}^{N-1} \frac{\partial}{\partial x_r} \{ q^{(r)}(x_r) P(\vec{x}, t) \} \quad (15)$$

where,

$$\begin{aligned} s^{(r)}(x_r) &= \begin{cases} \frac{\Omega}{2} \left\{ \left(\gamma_1^{(r)} \right)^2 x_r^2 - 2c_r \gamma_1^{(r)} \gamma_2^{(r)} x_r + \left(\gamma_2^{(r)} \right)^2 \right\} & c_r \in [-1, 1] \\ \frac{\Omega}{2} \left\{ \left(\gamma_1^{(r)} \right)^2 x_r^2 - 2c_r \gamma_1^{(r)} \gamma_2^{(r)} x_r + \left(\gamma_2^{(r)} \right)^2 (2c_r^2 - 1) \right\} & c_r \in \mathbb{R}/[-1, 1] \end{cases} \\ q^{(r)}(x_r) &= \omega^{(r)} - \sigma \lambda_r x_r \end{aligned} \quad (16)$$

Here $s^{(r)}$ represents a diffusion matrix and $q^{(r)}$ a drift vector. In the form Eq.(15), the diffusion matrix has been diagonalised.

3. Solving the Fokker-Planck equations

3.1. Outline of solution method

In the following, we sketch out the method of solving the Fokker-Planck equations in order to present relatively quickly the final solutions. Detailed derivations are given in the appendices.

Due to the diagonal form of the diffusion matrix, we decompose $P(\vec{x}, t)$ into a product of $N - 1$ terms,

$$P(\vec{x}, t) = \prod_{r=1}^{N-1} P_r(x_r, t)$$

so that Eq.(15) decouples into separate equations for each r

$$\begin{aligned} \frac{\partial}{\partial t} P_r(x_r, t) &= \frac{\partial^2}{\partial x_r^2} \{s^{(r)}(x) P_r(x_r, t)\} - \frac{\partial}{\partial x_r} \{q^{(r)}(x) P_r(x_r, t)\} \\ P_r(x_r, t') &= \delta(x_r - x'_r) \end{aligned} \quad (17)$$

for $r = \{1, \dots, N-1\}$. Since we have decoupled the modes we shall drop the sub(super)scripts r from this point on. Solving Eq.(17) is the main concern for the remainder of this paper.

3.2. Stationary densities

We first solve for the *stationary density* of Eq.(17), denoted $P_{\text{st}}(x)$, by setting $\frac{\partial}{\partial t} P(x, t) = 0$. We obtain the corresponding (Pearson's) differential equation,

$$\frac{d}{dx} \{s(x) P_{\text{st}}(x)\} - q(x) P_{\text{st}}(x) = 0.$$

Being linear its solution is

$$P_{\text{st}}(x) = \frac{1}{s(x)} \exp \left\{ \int dx \frac{q(x)}{s(x)} \right\}. \quad (18)$$

P_{st} is also referred to as a weight function. Substituting the product

$$P(x, t) = P_{\text{st}}(x) g(x, t) \quad (19)$$

into Eq.(17), the ensuing equation for $g(x, t)$ is

$$\frac{\partial}{\partial t} g(x, t) = s(x) \frac{\partial^2}{\partial x^2} g(x, t) + q(x) \frac{\partial}{\partial x} g(x, t). \quad (20)$$

We identify a Sturm-Liouville operator

$$\mathcal{H} = -s(x) \frac{d^2}{dx^2} - q(x) \frac{d}{dx}. \quad (21)$$

The factor $g(x, t)$ can thus be decomposed in terms of the normal modes of \mathcal{H}

$$\mathcal{H}u_\xi(x) = \xi u_\xi(x), \xi \neq 0. \quad (22)$$

The eigenvalues ξ may be discrete or continuous depending on boundary conditions, to be specified explicitly below. Then the full probability distribution can be expressed, as usual, in terms of these eigenfunctions and eigenvalues

$$P(x, x'|t, t') = P_{\text{st}}(x) \sum_{\xi} \rho_{\xi} e^{-\xi(t-t')} u_{\xi}(x) u_{\xi}^*(x')$$

where the sum will be an integral for the continuous parts of the spectrum, and constants ρ_{ξ} should be determined so that the initial condition at $t = t'$

$$P(x, x'|t', t') = \delta(x - x')$$

is satisfied.

3.3. Exact solutions to Fokker-Planck equations

In contrast to [14], we can go somewhat further than the stationary parts and solve - in some cases - the time dependence. Here we lay out the structure of that solution for the cases we have successfully solved.

Determining the nature of the spectrum of eigenvalues ξ and eigenfunctions u_{ξ} are the boundary conditions in x, x' - oscillatory or non-oscillatory - which in turn relate to the order of the coefficient polynomial $s(x)$. From Eq.(16), $s(x)$ is either a constant ($\gamma_1^{(r)} = 0$) or a quadratic polynomial ($\gamma_1^{(r)} \neq 0$). Three cases of boundary conditions are relevant:

- *Case I:* Non-oscillatory at boundaries, $s(x)$ constant: the spectrum is entirely discrete and the eigenfunctions u are Hermite polynomials. [16].
- *Case II:* Oscillatory at one boundary, $s(x)$ quadratic: the spectrum is mixed, with the discrete eigenvalues associated with Bessel polynomials [17] as eigenfunctions u and eigenfunctions for the continuous spectrum are the Whittaker functions.

- *Case III*: Oscillatory at both boundaries, $s(x)$ quadratic: the spectrum is again mixed. For this case, however, we have not been able to satisfactorily solve the full time-dependence (although we know the eigenfunctions u for the discrete spectrum are the Romanovski polynomials [18]). We shall only give the stationary density for this case.

So that the reader can readily see the overall form of the solutions, we present them here without detailed derivation.

3.3.1. Case I

In terms of a variable $z = \sqrt{\sigma\lambda/\Omega}(x - \omega/\sigma\lambda)$, the probability density function for this case is given in terms of Hermite polynomials $H_n(z)$:

$$P^{(I)}(z, z'|t, t') = \sqrt{\frac{\sigma\lambda}{\pi\Omega\gamma_2^2}} e^{-z^2} \sum_{n=0}^{\infty} \frac{1}{2^n n!} e^{-\sigma\lambda n(t-t')} H_n(z) H_n(z') \quad (23)$$

The prefactor originates from the stationary part of the distribution,

$$P_{\text{st}}^{(I)} = \sqrt{\frac{\sigma\lambda}{\pi\Omega\gamma_2^2}} e^{-z^2}. \quad (24)$$

After applying the Mehler formula for Hermite polynomials (see Appendix F) the final form of the probability density becomes,

$$P^{(I)}(x, x'|t, t') = \sqrt{\frac{\sigma\lambda}{\pi\gamma_2^2\Omega(1 - e^{-2\sigma\lambda(t-t')})}} \exp \left\{ -\frac{\sigma\lambda}{\gamma_2^2\Omega(1 - e^{-2\sigma\lambda(t-t')})} \times \left(x - x' e^{-\sigma\lambda(t-t')} - \frac{\omega}{\sigma\lambda} (1 - e^{-\sigma\lambda(t-t')}) \right)^2 \right\}. \quad (25)$$

We recognise this as a Gaussian smearing around the deterministic solution, Eq.(7). In the appendix we show that for $\Omega \rightarrow 0$ this becomes a delta function concentrated about Eq.(7).

3.3.2. Case II

Here the probability density function is given in terms of the Bessel polynomials and Whittaker functions (here expressed as ${}_2F_0$ functions):

$$P^{(II)}(x, x'|t, t') = \frac{|\gamma_1|}{\beta_2^{\beta_1+1}} z^{\beta_1} e^{-\frac{\beta_2}{z}} \left[\sum_{0 \leq n < -\frac{\beta_1+1}{2}} \frac{(-2n - \beta_1 - 1)}{n! \Gamma(-n - \beta_1)} e^{\frac{\Omega\gamma_1^2}{2} n(n+\beta_1+1)(t-t')} \right]$$

$$\begin{aligned}
& \times B_n^{(\beta_1, \beta_2)}(z) B_n^{(\beta_1, \beta_2)}(z') \\
& + \int_0^\infty d\mu \frac{\Gamma\left(\frac{\beta_1+1}{2} + i\mu\right) \Gamma\left(\frac{\beta_1+1}{2} - i\mu\right)}{2\pi\Gamma(i\mu)\Gamma(-i\mu)} e^{-\frac{\Omega\gamma_1^2}{2}\left(\frac{(\beta_1+1)^2}{4} + \mu^2\right)(t-t')} \\
& \times \psi(\mu, z)\psi(\mu, z') \Big]
\end{aligned} \tag{26}$$

where $z = \gamma_1 x - \gamma_2$ and $z' = \gamma_1 x' - \gamma_2$,

$$\beta_1 = -\frac{2\sigma\lambda}{\Omega\gamma_1^2} - 2, \quad \beta_2 = \frac{2}{\Omega\gamma_1} \left(\omega - \frac{\sigma\lambda\gamma_2}{\gamma_1} \right) \tag{27}$$

and

$$\psi(\mu, z) = {}_2F_0 \left(\frac{\beta_1+1}{2} - i\mu, \frac{\beta_1+1}{2} + i\mu \middle| -\frac{z}{\beta_2} \right). \tag{28}$$

Unfortunately, no corresponding simplification of this via a Mehler formula is possible. The stationary part that leads to Eq.(26) is,

$$P_{\text{st}}^{(II)}(x) = \frac{|\gamma_1|}{\beta_2^{\beta_1+1}} \frac{(-\beta_1-1)}{\Gamma(-\beta_1)} z^{\beta_1} e^{-\frac{\beta_2}{z}}. \tag{29}$$

3.3.3. Case III

Our efforts for this case have not satisfactorily led to formulae analogous to Eq.(26). However the stationary density is straightforwardly derived. We redefine z, β_1 and β_2 for this case as $z = \frac{1}{\sqrt{|1-c^2|}} \left(\frac{\gamma_1}{\gamma_2} x - c \right)$ (and similarly for z'), and

$$\beta_1 = -\frac{\sigma\lambda}{\Omega\gamma_1^2} - 1, \quad \beta_2 = \frac{2}{\Omega\gamma_1^2\sqrt{|1-c^2|}} \left(\frac{\omega\gamma_1}{\gamma_2} - \sigma\lambda c \right). \tag{30}$$

The stationary density is then,

$$P_{\text{st}}^{(III)}(z) = \frac{|\gamma_1|}{|\gamma_2|\sqrt{|1-c^2|}} \frac{(z^2+1)^{\beta_1} e^{\beta_2 \arctan(z)}}{\int_{-\frac{\pi}{2}}^{\frac{\pi}{2}} d\theta \frac{e^{\beta_2 \theta}}{(\cos\theta)^{2(\beta_1+1)}}}. \tag{31}$$

These are the solutions of the Fokker-Planck equations, including the time-dependence of the probability distribution functions for two out of three of the cases. Armed with these, we examine the stability question.

4. Stability considerations

Recall that deterministic stability of the phase synchronised fixed point is characterised by the condition that, when initial fluctuations are small and the coupling sufficiently large then under time evolution the system remains in the vicinity of the fixed point, Eq.(9). Here, if for some modes r this condition is not satisfied then deterministic trajectories will drive the system away from phase synchronicity. Now, in the presence of noise the system is no longer described by a single point but by a diffuse region governed by the probability density $P(\vec{x}, t)$ which is a solution to the Fokker-Planck equation Eq.(15). Using the graph Laplacian, we represent this as a region in the multi-dimensional space with axes x_r through the product form $P(\vec{x}, t) = \prod_r P_r(x_r, t)$. Following Schuss [10], we determine now whether the system can diffuse beyond the basin of attraction for some particular mode r , namely whether there is a finite probability - as determined from the solutions now to Eq.(17) - that $|x_r(t)| > 1$. When such modes occur, phase synchronicity can be said to be stochastically unstable. Moreover, where we have access to the complete time-dependence (and not just stationary distributions) we can determine whether some solutions to the truncated equations leave the region $|x_r| \ll 1$ in *finite* time; in other words, there may be cases of instability that the stationary distributions do not detect.

4.1. Case I

For the case of $\gamma_1 = 0$, as we can see in the time-dependence of Eq.(25), the stochastic system tracks the deterministic system which itself is stable, never departing from the basin of attraction of the fixed point x^* defined in Eq.(8). We can also see from the stationary part of the probability distribution Eq.(24) that the peak is determined from

$$\frac{d}{dx} P_{\text{st}}^{(I)} = 0 \Rightarrow x_{\text{peak}}^{(I)} = \frac{\omega}{\sigma\lambda} = x^*.$$

We can go further and track the movement of the density peak of the diffusing system with respect to time using,

$$\frac{d}{dx} P^{(I)}(x, x'|t, t') = 0 \Rightarrow x = x' e^{-\sigma\lambda(t-t')} + \frac{\omega}{\sigma\lambda} \left(1 - e^{-\sigma\lambda(t-t')}\right).$$

For small diffusion constant Ω the phase synchronicity is therefore effectively stable. The tail of the distribution, however, extends outside the region

$|x_r| \ll 1$. But from Eq.(25), the probability of the diffusing system escaping the fixed point is exponentially suppressed. Thus stochastic fluctuations on the frequencies alone ($\gamma_1 = 0$) do not significantly destabilise phase synchronicity.

4.2. Case II

In this case, we cannot so easily read off the final distribution Eq.(26) whether there is a probability that the system will leave the regime $|x_r| \ll 1$. In the section below we will plot various cases which will give more insight into the evolution of the probability distributions. Analytically, we can again locate the peak of the stationary probability distribution from Eq.(29):

$$\frac{d}{dx} P_{\text{st}}^{(II)}(x) = 0 \Rightarrow x_{\text{peak}}^{(II)} = \frac{\left(\frac{\omega}{\sigma\lambda} + \frac{\Omega\gamma_1\gamma_2}{\sigma\lambda}\right)}{1 + \frac{\Omega\gamma_1^2}{\sigma\lambda}} = \frac{\left(x^* + \frac{\Omega\gamma_1\gamma_2}{\sigma\lambda}\right)}{1 + \frac{\Omega\gamma_1^2}{\sigma\lambda}}. \quad (32)$$

We thus see that the peak is shifted compared to the deterministic fixed point. However, noting that the denominator of Eq.(32) is always greater than one, the only means for $x_{\text{peak}}^{(II)}$ to exceed one (for a strong instability) is if $\gamma_1\gamma_2$ are sufficiently large. In particular, this means that stochastic fluctuations of the coupling alone ($\gamma_2 = 0$) give

$$x_{\text{peak}}^{(\gamma_2=0)} = \frac{x^*}{1 + \frac{\Omega\gamma_1^2}{\sigma\lambda}} < 1.$$

In this case, the tail can extend beyond $|x| = 1$ but, for sufficiently small Ω , the probability that the system can drift from the basin of attraction is suppressed by a combination of exponential and power-law factors, as can be read off the large z properties of Eq.(29).

Evidently, given that increasing γ_1 will increase the denominator of Eq.(32) more than the numerator, the parameter γ_2 is the most effective means for pushing the peak of the distribution past $x = 1$. The coefficient of the stochastic fluctuations of the frequencies, while also maintaining fluctuations of the coupling, is the effective means of driving the system into instability.

4.3. Case III

We can again locate the peak of the stationary probability distribution from Eq.(31):

$$\frac{d}{dx} P_{\text{st}}(x) = 0 \Rightarrow x_{\text{peak}}^{(III)} = \frac{\left(x^* + c\frac{\Omega\gamma_1\gamma_2}{\sigma\lambda}\right)}{1 + \frac{\Omega\gamma_1^2}{\sigma\lambda}}. \quad (33)$$

The noise correlation parameter c becomes an additional degree of freedom for driving instability, with $c > 1$ for fixed γ_1 and γ_2 . However, even with the peak of the distribution lying in the basin $x < 1$, the tail of the distribution is different from cases I and II. Noting that the leading behaviour in a Taylor expansion of $e^{\beta_2 \arctan z}$ is a *constant*, the behaviour of the stationary distribution for large x is purely power-law,

$$P_{\text{st}}^{(III)}(x) \propto (1/x^2)^{1 + \frac{\sigma\lambda}{\Omega\gamma_1^2}}.$$

This power-law dependence for the correlated case means that the suppression is considerably weaker than for the previous cases.

We conclude therefore that increased correlation between noise in coupling and frequencies is the main driver of stochastic instability from phase synchronisation.

5. Probability Density Plots

When the noise is correlated we have been unable to infer directly from the analytic form of the probability distributions whether the system can be driven from the basin of the fixed point in finite time, and have thus relied on stationary limits. For the cases where we have solved the time-dependence we plot several cases to check this possibility.

To place the stochastic dynamics back into the network context we use a case considered by one of us previously in [7] for which synchronisation properties of the deterministic system are known. We use a small-scale $N = 27$ node variation on the Ravasz-Barabasi (RB) graph [19] that combines elements of hierarchy and randomness. In Fig.1 we show the graph in a circular embedding and a plot of the spectrum of its Laplacian eigenvalues. The four low-lying eigenvalues are $\lambda_1 = 0.586, \lambda_2 = \lambda_3 = 0.764, \lambda_4 = 0.944$.

We also used, in [7], a set of intrinsic frequencies ω_i drawn from a uniform distribution in the range $\omega_i \in [0, 1]$; the choice of maximum value of order unity fixes a free scale of the model. Fig.2 shows the particular frequencies used in this case. For these frequencies, the largest values of the ratio $\rho_r = \omega^{(r)}/\lambda_r$ (which determines the fixed point) are $\rho_4 = 0.530, \rho_1 = 0.339, \rho_3 = 0.241$. Note that both $r = 1, 4$ correspond to eigenvectors with all non-zero components while, for example, $\nu^{(3)} = (0_5, -1.236, -1_4, 0_5, 1.236, 1_4, 0_7)$ where x_n here means that the n sequential components have value x . We

therefore examine this mode, $r = 3$, because it involves fewer participating nodes. The corresponding projection of the frequency vector onto this eigenvector is $\omega^{(3)} = 0.1843$.

According to first order considerations of the deterministic system [7], for all couplings $\sigma > \rho_4 = 0.53$ the system should be stably locked in a state of global phase synchrony. Numerical calculations confirm this [7]. In fact, this behaviour extends down to coupling of $\sigma = 0.212$ whereupon the system exhibits semi-stable periodic behaviour (consistent with the second order considerations of [7]).

We therefore know that the deterministic system has a stable phase synchronised fixed point at a coupling, say, of $\sigma = 0.8$. We examine the effect of noise on the $r = 3$ Laplacian mode. On this basis, we expect a valid fixed point at $x^* = \rho_3/\sigma = 0.3$. The initial configuration is also taken in the vicinity of the fixed point, $x' = -0.2$ (we use a negative initial value to give scope for the probability distribution to detectably shift in the narrow interval $x \in [-1, 1]$). We take the diffusion constant to be $\Omega = 0.1$ and use an initial delta function at $t' = 0$.

We consider three cases, one with purely additive noise and two combining additive and multiplicative noise:

- Case I: $\gamma_1 = 0, \gamma_2 = -2$, for which the Sturm-Liouville operator Eq.(21) has a purely discrete spectrum with the Hermite polynomials as eigenfunctions;
- Case II.1: $\gamma_1 = 2, \gamma_2 = -2$, which involves a mixed spectrum of Eq.(21) and Bessel polynomials; and
- Case II.2: $\gamma_1 = 2, \gamma_2 = -7$, with a similar analytic structure to the previous choice.

Because we do not have access, at this stage, to the time-dependence for Case III we shall instead compare the stationary distributions across these cases with the given graph structure and frequency spectrum. We thus compare the stationary limits of the above three choices with the following correlated choices:

- Case III.1: $\gamma_1 = 2, \gamma_2 = -2$ and $c = 1.1$;
- Case III.2: $\gamma_1 = 2, \gamma_2 = -2$ and $c = 0.9$; and

- Case III.3: $\gamma_1 = 2, \gamma_2 = -2$ and $c = 0.2$.

Using $P^{(I)}$ given in Eq.(25) with the following parameter values

$$\omega = 0.184, \sigma = 0.8, \lambda = 0.764, \gamma_1 = 0, \gamma_2 = -2, \Omega = 0.1, x' = -0.2.$$

The $t = 0$ plot in Fig.3 is close to a delta function at $x = -0.2$, reflecting the choice of initial condition. As time progresses the peak of the distribution moves to the right as the distribution flattens out, finally reaching its stationary shape concentrated around $x = \frac{\omega}{\sigma\lambda} = 0.3$, reflecting the $t \rightarrow \infty$ limit of Eq.(7). For this choice of parameters, the tail evidently extends across the boundary $x = 1$ but the strong (exponential) suppression is also manifest. Naturally, smaller values of the diffusion constant Ω suppress this further.

Using $P^{(II)}$ given in Eq.(26) with the following parameter values

$$\omega = 0.184, \sigma = 0.8, \lambda = 0.764, \gamma_1 = 2, \gamma_2 = -2, \Omega = 0.1, x' = -0.2.$$

leads to the evolving probability density shown in Fig.4. Near $t = 0$ the curve is visibly close to the initial delta function shape around $x = -0.2$. As time progresses the peak of the distribution broadens, becomes asymmetric but does not shift significantly. This is because the distribution reaches its stationary ($t = \infty$) shape with a peak at $x = -0.21$, close to its starting point and consistent with Eq.(32) (and Eq.(33) with $c = 1$). The distribution is strongly suppressed for negative values, consistent with its asymmetry. The suppression is less severe for positive values of x , though not easily seen in the plot, with still with no significant support for $x > 1$.

Using again Eq.(26) now with the parameter values

$$\omega = 0.184, \sigma = 0.8, \lambda = 0.764, \gamma_1 = 2, \gamma_2 = -7, \Omega = 0.1, x' = -0.2.$$

we obtain the evolving density in Fig.5. We now observe a distinct shift to the left from the initial delta function at $x = -0.2$, with the density becoming asymmetric and settling into the stationary configuration with peak at $x = -1.2$, consistent with Eq.(32). The peak is evidently outside the region $|x| < 1$. Moreover, the tail of the distribution is ‘fat’, evidently ‘spilling’ across the boundary $x > 1$ with weaker suppression than before.

We note overall that the shifts in the distributions as time evolves do not show multiple ‘bounces’ across the interval $|x| \leq 1$, rather a monotonic evolution from the initial configuration to the stationary distribution. Indeed, even with small noise the distributions become too diffuse to allow any

discernment of changes of direction of the system within the narrow bounds of the region $|x| < 1$ from subsets of trajectories. Therefore, if the stationary density has a peak lying inside the interval $|x| \leq 1$ then for all intermediate times the support of the distribution will also lie in this domain. Then stochastic instability can be concluded from the stationary density.

Finally, we compare in Fig.6 the (appropriately normalised) stationary densities across all the cases, including those with correlated noise. We observe, consistent with the above time-dependent plots and our analytic results, that as we move to more and more complex combinations of noise, both additive and multiplicative, the position of the peaks of the long time distributions move outside the basin of attraction $|x| < 1$. However, the height of the peaks reduces and the degree of smearing increases. We also observe a smooth transition between the curves from Case II to Case III. Though we do not plot it, increasing $c > 1$ further suppresses the height of the peak and smears the support of the distribution across broad regions of values of x .

6. Summary and Discussion

We have demonstrated the circumstances under which instabilities can be generated by stochastic fluctuations in the Kuramoto model of oscillators coupled on a general network. This was achieved by applying both additive and multiplicative noise to the dynamical equations linearised in the vicinity of the phase synchronised fixed point where the equations can be decoupled into eigenmodes of the graph Laplacian of the underlying network. With the noise the dynamics is no longer strictly deterministic but is described probabilistically. In a number of cases, we exactly solved for the time-dependent probability density function for each Laplacian mode of the system. However, the stationary densities provided sufficient information to determine the stability of the system.

For sufficiently large diffusion constant the tails of the probability distributions always extend beyond the deterministically defined fixed point basin of attraction and provide for a finite probability that the mode can drift from conditions consistent with synchronicity. However even for small values of the diffusion constant correlation between stochastic fluctuations of the frequencies and coupling generate a significant mechanism for instability. Firstly, suppression of the probability outside the basin of attraction is weaker as the distribution tail changes from being exponential to power-law. We may call

this a weak stochastic instability. More pronouncedly, correlation of noise allows the peak of the stationary distribution to be shifted outside the basin of attraction. In this case, trajectories will escape the basin of attraction with probability of order one rendering the system strongly stochastically unstable.

We have thus far avoided limiting our calculations to particular networks popularly used in the literature or particular frequency distributions. We can now make some broad statements about such cases while treating the frequency distribution as fixed. As mentioned at the outset, for deterministic systems on easily disconnected graphs larger coupling is needed to stabilise phase synchronisation due to the ratio $\frac{\omega^{(r)}}{\sigma\lambda_r}$. With noise now, we note that in determining the peak of the stationary density for generally correlated noise with Eq.(33), the stochastic parameter combination $c\Omega\gamma_1^{(r)}\gamma_2^{(r)}$ is played off against the deterministic system combination $\sigma\lambda_r$. Thus larger values of the latter combination (strong coupling or high connectivity of the graph) can be overcome by larger values of the stochastic parameters to drive instability. Conversely, small values of the stochastic parameters suffice to de-stabilise easily disconnected graphs. However there is no ‘free lunch’. Since low-lying modes $r \sim 1$ for poorly connected graphs ($\lambda_r < 1$) typically have a larger number of nodes in the corresponding eigenvector $\nu^{(r)}$, the noise must be manifested in a large number of nodes for the system to be stochastically unstable. Depending on the nature of the system and whether stability is desired or undesired, it may be expensive to ‘attack’ or ‘defend’ many nodes.

The balancing point of stochastic instability is somewhere in the middle: graphs whose distribution of Laplacian eigenvalues exhibits a ‘bulk’ around $\lambda_r \sim 1$ for $1 \ll r \ll N - 1$, namely graphs with a large number of subgraphs that can be disconnected by a small number of link removals. This is the case for sparse Erdős-Rényi and Scale-Free graphs [20]. Such graphs are therefore easily susceptible to stochastic instability. Contrastingly [20], dense Erdős-Rényi (if generated with high rewiring probability from a regular graph) and Small World graphs have Laplacian spectra with the bulk of eigenvalues shifted away from $\lambda_r = 1$. These graphs are thus less susceptible to stochastic instability. For the Small-World case this applies even for low re-wiring probability, because even then the bulk of the Laplacian spectrum is shifted away from $\lambda_r \sim 1$. This mirrors the strong synchronisability properties of the Small-World graph observed by [21]. Our analytic results, such as the positions of peaks of probability distributions, are sufficiently straightforward that the ‘weak points’ - those nodes significant in determining the transition

to stochastic instability - can be easily computed for any network of interest.

It is difficult to find a precedent for our results in the literature given the limited cases that have been investigated. For identical frequencies and a complete graph, Park and Kim [8] showed that noisy coupling - or multiplicative noise - can induced non-trivial behaviours: a transition of the synchronised properties of the system from there being one to two clusters. Combining additive and multiplicative noise in the completely connected identical oscillator case leads to even richer behaviours, with the former able to suppress the effects of the latter as well as inducing saddle-node bifurcations [9]. In our case, we have been able to go further than [8, 9] in analysing stability of any network that can be described by an adjacency matrix. On the other hand, apart from identifying conditions for instability we cannot say more than these authors about alternative stable or meta-stable states (for example we cannot see in Eq.(33) a mechanism for mutual cancellation between noisy coupling and frequencies, as observed by [9]). We also note that both [8, 9] use additional ‘pinning’ terms not found in the original Kuramoto model.

To make more specific statements about transitions from phase synchronicity to alternative fixed points or meta-stable states requires stochastically probing beyond the first order approximations treated here. For example, in our earlier work [7] we observed that second order approximations promoted the ‘population model’ analogue to the Kuramoto model from the logistic to the Lotka-Volterra equations. This offers the tantalising possibility of exploiting work on the impact of noise on multi-species competition dynamics to make more precise conclusions about phase synchronisation.

Acknowledgements

The authors are grateful to Murray Batchelor, Richard Taylor, Tony Dekker and Markus Brede for invaluable discussions and comments. This work was supported through the Internship program of the Australian Mathematical Sciences Institute (AMSI) and the Brazilian research agency FAPESP.

Appendix A. Properties of the Graph Laplacian

We repeat here the definition of the graph Laplacian [11] for a graph G :

$$L_{ij} = D_{ij} - A_{ij}$$

where A_{ij} is the graph adjacency matrix and D_{ij} is the diagonal matrix of degrees $d_i = \sum_j A_{ij}$.

The spectrum of Laplacian eigenvalues λ_r , $r = 0, \dots, N-1$, is positive semi-definite

$$\lambda_0 = 0 \leq \lambda_1 \leq \lambda_2 \leq \dots \leq \lambda_{N-1}$$

as can be proven using the Rayleigh-Ritz ratio for symmetric matrices [11].

The degeneracy of the zero eigenvalue corresponds to the number of disconnected components into which the graph can be separated. For a connected graph forming a single component the eigenvector corresponding to the (now) non-degenerate zero mode is easily seen to be

$$\nu^{(0)} = \frac{1}{\sqrt{N}}(1, \dots, 1).$$

The first non-zero eigenvalue is known as the Fiedler [12] and encodes important properties of the graph. It is also known as the algebraic connectivity [11] and provides a lower bound on the variety of measures of connectivity of G :

$$\lambda_1(G) \leq \kappa(G) \leq \lambda(G) \leq \delta(G) \leq (d_i, \bar{d}) \leq \Delta(G) \quad (\text{A.1})$$

where $\kappa(G)$ is the vertex connectivity (the minimum number of vertices that need to be removed to disconnect the graph), $\lambda(G)$ the edge connectivity (minimum number of edges to be removed to disconnect the graph), $\delta(G)$ the minimal degree and $\Delta(G)$ the maximal degree of the graph.

Mohar [22] summarises a range of theorems about the spectrum of the Laplacian and relationships between it and invariant distance measures. Chung [23], using a variation known as the ‘analytic Laplacian’, proves that the distance between any two subsets in G is bounded from above by a function of the lowest and highest eigenvalues.

Appendix B. Deterministic limits of the stochastic system

Recall that the logistic-like Eq.(6) with initial condition, $x_r(t') = x'_r$ can be solved exactly, with solution

$$x_r(t) = x'_r e^{-\sigma \lambda_r (t-t')} + \frac{\omega^{(r)}}{\sigma \lambda_r} \left(1 - e^{-\sigma \lambda_r (t-t')} \right). \quad (\text{B.1})$$

We refer to this as the deterministic solution to the stochastic system. This result can be arrived at from within the stochastic system using both the Langevin and Fokker-Planck equations.

The exact solution to the corresponding Langevin equation is given by,

$$x_r(t) = e^{-\sigma\lambda_r t - \gamma_1^{(r)} \int dt \Gamma_r^{(m)}(t)} \\ \times \left\{ \int^{t_1=t} dt_1 \left(\omega^{(r)} + \gamma_2^{(r)} \Gamma_r^{(a)}(t_1) \right) e^{\sigma\lambda_r t_1 + \gamma_1^{(r)} \int^{t_2=t_1} dt_2 \Gamma_r^{(m)}(t_2)} + k_r \right\}$$

and the integration constant, k_r , is given by,

$$k_r = x'_r e^{\sigma\lambda_r t' + \gamma_1^{(r)} \int^{t=t'} dt \Gamma_r^{(m)}(t)} \\ - \int^{t_1=t'} dt_1 \left(\omega^{(r)} + \gamma_2^{(r)} \Gamma_r^{(a)}(t_1) \right) e^{\sigma\lambda_r t_1 + \gamma_1^{(r)} \int^{t_2=t_1} dt_2 \Gamma_r^{(m)}(t_2)}.$$

We observe that the zero limit of all γ parameters gives back the deterministic result Eq.(7).

We can also see the deterministic result arising from the solutions to the Fokker-Planck equation as Ω approaches zero. This statement can be elegantly demonstrated in the pure stochastic frequency case, where the probability density is given initially through the Hermite polynomials. Starting with the expression Eq.(25) for the density after use of the Mehler formula and applying the following delta function identities,

$$\delta(x) = \lim_{\epsilon \rightarrow 0^+} \frac{1}{\sqrt{\pi\epsilon}} \exp\left(-\frac{x^2}{\epsilon}\right), \quad \delta(ax) = \frac{1}{|a|} \delta(x), \quad a \in \mathbb{R}$$

we obtain,

$$\lim_{\Omega \rightarrow 0^+} P(x, x'|t, t') = \delta\left(x - x' e^{-\sigma\lambda\bar{t}} - \frac{\omega}{\sigma\lambda} \left(1 - e^{-\sigma\lambda\bar{t}}\right)\right).$$

The result is a pure Dirac delta function about the deterministic trajectory. We also note that

$$\langle x \rangle = x' e^{-\sigma\lambda\bar{t}} + \frac{\omega}{\sigma\lambda} \left(1 - e^{-\sigma\lambda\bar{t}}\right)$$

so that the expectation value of x tracks the deterministic trajectory.

Appendix C. Spectral categories for Fokker-Planck equations

Following the work of Linetsky [24], we detail the form of $g(x, t)$ which are solutions to Eq.(20), the remaining part of the Fokker-Planck equation after separation of the stationary solution. This solution depends on the detailed form of the functions $q(x)$ and $s(x)$ and the range of x .

Consider the Sturm-Liouville operator Eq.(21), and the associated eigenvalue problem Eq.(22), namely

$$s(x)\frac{d^2}{dx^2}u(x) + q(x)\frac{d}{dx}u(x) + \xi u(x) = 0, \quad \xi \geq 0 \quad (\text{C.1})$$

where the range of x for Eq.C.1 is given by $x \in [x_{\min}, x_{\max}]$. Let e be an end-point of this range, namely $e \in \{x_{\min}, x_{\max}\}$.

If $e \neq \pm\infty$ then Eq.(C.1) is classed as non-oscillatory for all ξ . If $e = \pm\infty$, referred to as a *natural boundary*, then we must examine more closely. Transforming the variable x and the solution $u(x)$ via the following,

$$y(x) = \int \frac{dx}{\sqrt{s(x)}}, \quad v(y) = u(x(y)) [W(x(y))]^{\frac{1}{2}} [s(x(y))]^{\frac{1}{4}} \quad (\text{C.2})$$

the corresponding Sturm-Liouville equation for $v(x(y))$ becomes the one-dimensional Schrödinger equation with the potential,

$$\begin{aligned} V(x) = & \frac{1}{4} \left(\frac{d}{dx} \sqrt{s(x)} \right)^2 - \frac{1}{2} \sqrt{s(x)} \frac{d^2}{dx^2} \sqrt{s(x)} + \frac{1}{4} \frac{q^2(x)}{s(x)} + \frac{1}{2} \frac{d}{dx} q(x) \\ & - \frac{q(x) \frac{d}{dx} \sqrt{s(x)}}{\sqrt{s(x)}} \end{aligned} \quad (\text{C.3})$$

The classification at the natural boundary is then given by the following theorem.

Theorem *Classification at natural boundaries (Linetsky).*

- If e is transformed into a finite endpoint under Eq.(C.2), namely $y(e) \neq \pm\infty$, then Eq.(C.1) is classed as non-oscillatory for all ξ .
- If the transformed end-point is infinite, $y(e) = \pm\infty$, and $\lim_{x \rightarrow e} V(x) = \{\infty, 0\}$, then Eq.(C.1) is classed as non-oscillatory for all ξ .
- If for some finite non-vanishing $V(e)$, we have $\lim_{x \rightarrow e} V(x) = V(e)$, and $\lim_{x \rightarrow e} y^2(x)(V(x) - V(e)) > -\frac{1}{4}$, then Eq.(C.1) is classed as non-oscillatory for $\xi \in [0, V(e)]$ and oscillatory for $\xi > V(e)$.

We are now equipped to classify the exact forms of the solution to Eq.(20). More detail on these aspects can be found in section 4 of [24].

Appendix C.1. Spectral category I

If both boundaries exhibit no oscillatory behaviour, then the spectrum is purely discrete and the probability distribution is given by,

$$P(x, x'|t, t') = P_{st}(x) \sum_{n=0}^{\infty} e^{-\eta_n(t-t')} \rho_n \varphi_n(x) \varphi_n(x') , \rho_n \in \mathbb{R} \quad (\text{C.4})$$

where $\varphi_n(x)$, $n \geq 0$, are eigenfunctions according to

$$s(x) \frac{d^2}{dx^2} \varphi_n(x) + q(x) \frac{d}{dx} \varphi_n(x) + \eta_n \varphi_n(x) = 0 \quad (\text{C.5})$$

for the discrete eigenvalue η_n . Following Chap. 5 of [15], the spectrum is positive semi-definite:

$$\eta_n \in \mathbb{R} , 0 = \eta_0 < \eta_1 < \eta_2 < \dots$$

The eigenfunctions φ_n are the classical orthogonal polynomials, for specific forms of $s(x)$ and ranges of x :

- If $s(x)$ is a constant and $x \in \mathbb{R}$ then $\varphi_n(x)$ takes the form of a Hermite polynomial.
- If $s(x)$ is linear and $x \in \mathbb{R}_+$ then $\varphi_n(x)$ takes the form of a Laguerre polynomial.
- If $s(x)$ is quadratic with two distinct real roots and $x \in [-1, 1]$ then $\varphi_n(x)$ takes the form of a Jacobi polynomial.

These classical orthogonal polynomials come with the following *infinite orthogonality property*,

$$\int_{x_{min}}^{x_{max}} dx P_{st}(x) \varphi_n(x) \varphi_m(x) = \delta_{mn} h_n < \infty \text{ for } m, n = \{0, 1, 2, \dots\} \quad (\text{C.6})$$

indicating that the infinite set of eigenfunctions are square integrable with respect to the weight function P_{st} . In Appendix F we use the above orthogonality, and the initial condition $P(x, x'|t', t') = \delta(x - x')$ to obtain normalisation values, ρ_n , in Eq.(C.4).

Appendix C.2. Spectral category II

If one of the boundaries exhibits no oscillatory behaviour, with the other boundary exhibiting oscillatory behaviour for $\xi > V(e)$, then the probability density is given by,

$$P(x, x'|t, t') = P_{\text{st}}(x) \left[\sum_{n=0}^N e^{-\eta_n(t-t')} \rho_n \varphi_n(x) \varphi_n(x') \right. \\ \left. + P_{\text{st}}(x) \int_0^\infty d\mu e^{-\Lambda(\mu)(t-t')} \rho(\mu) \psi(\mu, x) \psi(\mu, x') \right]. \quad (\text{C.7})$$

We treat the discrete and continuous parts of this separately in the following.

Appendix C.2.1. On the discrete eigenvalues

For the finite sum term in Eq.(C.7), the eigenfunctions $\varphi_n(x)$ satisfy a differential equation equivalent to Eq.(C.5), with a corresponding discrete eigenvalue η_n , but where the orthogonal polynomials no longer exhibit the infinite orthogonality property Eq.(C.6), but a *finite orthogonality property*, namely

$$\int_{x_{\min}}^{x_{\max}} dx P_{\text{st}}(x) \varphi_n(x) \varphi_m(x) = \delta_{mn} h_n < \infty \quad m, n = \{0, 1, 2, \dots, N\} \quad (\text{C.8})$$

for finite integer N . We refer to these as *non classical* orthogonal polynomials. The cases of $s(x)$ which generate these polynomials are as follows:

- If $s(x)$ is quadratic with one repeated root and $x \in \mathbb{R}_+$ then $\varphi_n(x)$ takes the form of a Bessel polynomial.
- If $s(x)$ is quadratic with two distinct real roots and $x \in \mathbb{R}_+$ then $\varphi_n(x)$ takes the form of a Fisher-Snedecor polynomial.

Appendix C.2.2. On the continuous eigenvalue

For the continuous part of Eq.(C.7) we have the following eigenvalue equation for $\psi(\mu, x)$,

$$s(x) \frac{d^2}{dx^2} \psi(\mu, x) + q(x) \frac{d}{dx} \psi(\mu, x) + \Lambda(\mu) \psi(\mu, x) = 0 \quad (\text{C.9})$$

for the continuous eigenvalue $\Lambda(\mu)$. The integration variable μ provides a continuous index for the eigenvalue $\Lambda(\mu)$ (as n provides for the discrete value

η_n). Again, following Chap. 5 of [15] we have the following condition for the eigenvalue,

$$\Lambda(\mu) \in \mathbb{R} , \Lambda(\mu) > 0$$

The eigenfunction, $\psi(\mu, x)$, is a fundamental solution to Eq.(C.9) which is valid in the neighbourhood of the non-oscillatory boundary. The eigenfunctions for continuous eigenvalues must be orthogonal to eigenfunctions for the discrete η_n , $n \in \{0, \dots, N\}$.

The eigenvalue $\Lambda(\mu)$ can be found in one of two ways, from the finite orthogonality property or simply from considering the oscillatory cutoff point. Using the finite orthogonality approach (for the other method see [24]) we use the property Eq.(C.8), to infer the existence of a real number, \mathcal{J} , which is greater than the largest discrete eigenvalue, η_N ,

$$\eta_N < \mathcal{J}. \quad (\text{C.10})$$

If this is not the case then the finite orthogonality property (Eq.C.8) fails, leading to the catastrophic condition (specific details of this statement will be given in Appendix F), $h_n \rightarrow \infty$. Thus we define the continuous eigenvalue in the following way,

$$\Lambda(\mu) = \mathcal{J} + \kappa\mu^2 , \{\kappa, \mu\} > 0. \quad (\text{C.11})$$

We have necessarily that $\mathcal{J} = V(e)$. The choice of μ^2 for the dependence on the index μ in this parametrisation guarantees that the eigenvalue ranges from $[V(e), \infty]$.

The eigenfunctions with continuous eigenspectra are generally not polynomials but obey an equivalent orthogonality condition amongst themselves,

$$\int_{x_{min}}^{x_{max}} dx P_{st}(x) \psi(\mu, x) \psi(\nu, x) = \delta(\mu - \nu) h(\mu) \quad (\text{C.12})$$

and are completely orthogonal with their discrete spectrum counterparts,

$$\int_{x_{min}}^{x_{max}} dx P_{st}(x) \psi(\mu, x) \varphi_n(x) = 0 , n = \{0, 1, 2, \dots, N\} \quad (\text{C.13})$$

As with the first spectral category, the orthogonality conditions and the initial condition $P(x, x'|t', t') = \delta(x - x')$ are used to obtain the normalisation constants $\{\rho_n, \rho(\mu)\}$. Specific instances of these will be solved in Appendix F.

Appendix C.3. Spectral category III

If both boundaries exhibit oscillatory behaviour for some $\xi > \{V(-\infty), V(\infty)\}$ and $V(-\infty) = V(\infty)$ then the probability density is given by,

$$P(x, x'|t, t') = P_{\text{st}}(x) \left[\sum_{n=0}^N e^{-\eta_n(t-t')} \rho_n \varphi_n(x) \varphi_n(x') \right. \\ \left. + \sum_{ij=1}^2 \int_0^\infty d\mu e^{-\Lambda(\mu)(t-t')} \rho_{ij}(\mu) \psi_i(\mu, x) \psi_j(\mu, x') \right]. \quad (\text{C.14})$$

Note that there exist more general versions of spectral category III where $V(-\infty) \neq V(\infty)$, but we do not need to consider these in this work.

Appendix C.3.1. On the discrete eigenvalues

As with the previous spectral category, the eigenfunctions $\varphi_n(x)$ in Eq.(C.14) for the discrete eigenvalue η_n satisfy an equivalent differential equation to Eq.(C.5) and exhibit a finite orthogonality property Eq.(C.8). The relevant restriction for $s(x)$ for this spectral category is,

- If $s(x)$ is quadratic with two distinct complex roots and $x \in \mathbb{R}$ then $\varphi_n(x)$ takes the form of a Romanovski polynomial.

The continuous part of the spectrum continues to present some difficulties which is why we do not consider this case any further in this paper.

Appendix D. Properties of special functions for solving Fokker-Planck equations

In this section we give basic properties of the hypergeometric functions and differential equations used in our calculations. To begin we give some necessary definitions.

Appendix D.1. The Pochhammer symbol and Gamma functions

Two quantities we call upon extensively in the definition of hypergeometric functions are the Pochhammer symbol, $(x)_n$, and the Gamma function, $\Gamma(x)$, given by,

$$(x)_n = \prod_{j=0}^{n-1} (x+j) = \frac{\Gamma(x+n)}{\Gamma(x)}, \quad \Gamma(x) = \int_0^\infty dt e^{-t} t^{x-1}, \quad \Re(x) > 0.$$

Appendix D.2. Hypergeometric differential equations

In this work we consider hypergeometric differential equations of the form,

$$s(x) \frac{d^2}{dx^2} \psi(\mu, x) + q(x) \frac{d}{dx} \psi(\mu, x) + \Lambda(\mu) \psi(\mu, x) = 0 \quad (\text{D.1})$$

where,

- $s(x)$ is at most a quadratic polynomial of x
- $q(x)$ is a linear polynomial of x
- $\Lambda(\mu)$ the eigenvalue - is not a function of x .

Appendix D.3. Hypergeometric functions

Solutions to the above differential equation are referred to as hypergeometric functions, generally given as,

$${}_pF_q \left(\begin{matrix} a_1 & \dots & a_p \\ b_1 & \dots & b_q \end{matrix} \middle| x \right) = \sum_{j=0}^{\infty} \frac{(a_1)_j \dots (a_p)_j}{(b_1)_j \dots (b_q)_j} \frac{x^j}{j!}. \quad (\text{D.2})$$

In this work we are limited to $p = \{1, 2\}$ and $q = \{0, 1\}$. For more information see Chaps. 13, 14 and 15 of [16], and references therein.

Appendix D.4. Order n polynomials

Through the following choice for the eigenvalue,

$$\Lambda(\mu) = \eta_n = -n \left(\frac{d}{dx} q(x) + \frac{1}{2}(n-1) \frac{d^2}{dx^2} s(x) \right) \quad (\text{D.3})$$

the value of a_1 in Eq.D.2 becomes $-n$, and hence the series terminates at $j = n$, leading to a polynomial solution, $\varphi_n(x)$, of order n .

Appendix D.5. Weight functions

Each set of polynomials come equipped with a weight function, given by Pearson's differential equation,

$$\frac{d}{dx} \{s(x) P_{rmst}(x)\} - q(x) P_{st}(x) = 0 \Rightarrow P_{st}(x) = \frac{1}{s(x)} \exp \left\{ \int dx \frac{q(x)}{s(x)} \right\}.$$

Appendix D.6. Canonical forms

The following lists detail the canonical forms of $s(x)$, $q(x)$ and the weight functions of the six distinct cases of the previous section,

Polynomial	$s(\mathbf{x})$	$q(\mathbf{x})$	Eigenvalue
Hermite	1	$-2x$	$2n$
Laguerre	x	$\beta + 1 - x$	n
Jacobi	$1 - x^2$	$\beta_1 - \beta_2 - (\beta_1 + \beta_2 + 2)x$	$n(n + \beta_1 + \beta_2 + 1)$
Bessel	x^2	$(\beta_1 + 2)x + \beta_2$	$-n(n + \beta_1 + 1)$
Fisher-Snedecor	$x(x + 1)$	$(\beta_1 + \beta_2 + 2)x + \beta_1 + 1$	$-n(n + \beta_1 + \beta_2 + 1)$
Romanovski	$x^2 + 1$	$2(\beta_1 + 1)x + \beta_2$	$-n(n + 2\beta_1 + 1)$

Label	Interval	$P_{\text{st}}(\mathbf{x})$	Restrictions
$H_n(x)$	$x \in \mathbb{R}$	e^{-x^2}	
$L_n^{(\beta)}(x)$	$x \in \mathbb{R}_+$	$x^\beta e^{-x}$	$\beta > 0$
$P_n^{(\beta_1, \beta_2)}(x)$	$x \in [-1, 1]$	$(1+x)^{\beta_1}(1-x)^{\beta_2}$	$\{\beta_1, \beta_2\} > -1$
$B_n^{(\beta_1, \beta_2)}(x)$	$x \in \mathbb{R}_+$	$x^{\beta_1} e^{-\frac{\beta_2}{x}}$	$\beta_1 < 0, \beta_2 > 0, n^{(B)}$
$F_n^{(\beta_1, \beta_2)}(x)$	$x \in \mathbb{R}_+$	$x^{\beta_1}(1+x)^{\beta_2}$	$\beta_1 > -1, n^{(F)}$
$R_n^{(\beta_1, \beta_2)}(x)$	$x \in \mathbb{R}$	$(x^2 + 1)^{\beta_1} e^{\beta_2 \arctan x}$	$\beta_1 < 0, n^{(R)}$

Appendix D.6.1. On the restrictions

The interval of x refers to the region of integration necessary to satisfy the orthogonality conditions. Additionally, the restrictions $n^{(B)}$, $n^{(F)}$ and $n^{(R)}$ for the Bessel, Fisher-Snedecor and Romanovski cases respectively are,

$$\{n^{(B)}, n^{(F)}, n^{(R)}\} \Rightarrow \left\{ n < -\frac{\beta_1 + 1}{2}, n < -\frac{\beta_1 + \beta_2 + 1}{2}, n < -\left(\beta_1 + \frac{1}{2}\right) \right\}. \quad (\text{D.4})$$

These two conditions allude to the finite orthogonality conditions held by these sets of polynomials. We shall detail the derivation of these conditions shortly.

Appendix D.7. Rodrigues formula

Aside from solving the differential equation Eq.(C.5) directly, it is possible to obtain the explicit form of each order n polynomial using the so called *Rodrigues formula*,

$$\varphi_n(x) = C_n \frac{1}{P_{\text{st}}(x)s(x)} \frac{d^n}{dx^n} \{P_{\text{st}}(x)s^n(x)\} \quad \text{where } C_n \in \mathbb{R}. \quad (\text{D.5})$$

Appendix D.8. Orthogonality

We now detail the orthogonality of the polynomials. To do this we shall explicitly derive the infinite Eq.(C.6), and finite Eq.(C.8) orthogonality of the classical and non-classical polynomials respectively.

We begin by recasting Eq.(C.5) into the following form,

$$\frac{d}{dx} \left\{ s(x) P_{\text{st}}(x) \frac{d}{dx} \varphi_n(x) \right\} + \eta_n P_{\text{st}}(x) \varphi_n(x) = 0. \quad (\text{D.6})$$

Consider two copies of the above equation, one with index n and one with m , $m \neq n$. Multiply equation n with $\varphi_m(x)$, and multiply equation m with $\varphi_n(x)$. Finally, we subtract the two corresponding equations to obtain,

$$\begin{aligned} P_{\text{st}}(x) \varphi_n(x) \varphi_m(x) &= \frac{1}{\eta_n - \eta_m} \left[\varphi_n(x) \frac{d}{dx} \left\{ s(x) P_{\text{st}}(x) \frac{d}{dx} \varphi_m(x) \right\} \right. \\ &\quad \left. - \varphi_m(x) \frac{d}{dx} \left\{ s(x) P_{\text{st}}(x) \frac{d}{dx} \varphi_n(x) \right\} \right]. \end{aligned}$$

Integrating both sides with respect to x over the relevant intervals, and performing integration by parts to the right hand side we obtain,

$$\begin{aligned} \int_{x_{\min}}^{x_{\max}} dx P_{\text{st}}(x) \varphi_n(x) \varphi_m(x) &= \frac{1}{\eta_n - \eta_m} \left[s(x) P_{\text{st}}(x) \left\{ \varphi_n(x) \left(\frac{d}{dx} \varphi_m(x) \right) \right. \right. \\ &\quad \left. \left. - \left(\frac{d}{dx} \varphi_n(x) \right) \varphi_m(x) \right\} \right]_{x_{\min}}^{x_{\max}}. \quad (\text{D.7}) \end{aligned}$$

Appendix D.8.1. Infinite orthogonality

To illustrate the infinite orthogonality property of the classical orthogonal polynomials, consider the example of the Hermite polynomials. Inserting $\varphi_n(x) = H_n(x)$ into the right hand side of Eq.(D.7) we obtain,

$$\underbrace{\left[e^{-x^2} \left\{ H_n(x) \left(\frac{d}{dx} H_m(x) \right) - \left(\frac{d}{dx} H_n(x) \right) H_m(x) \right\} \right]_{x \rightarrow -\infty}^{x \rightarrow \infty}}_{\text{order } m+n-1 \text{ polynomial}}.$$

We notice that the order $m+n-1$ polynomial is completely suppressed by the weight function, e^{-x^2} , in the $x \rightarrow \pm\infty$ limit for all m and n , hence showing the infinite orthogonality of the Hermite polynomials. It is an equivalent process to show that the remaining classical polynomials have this property.

Appendix D.8.2. Finite orthogonality

To illustrate the finite orthogonality property of the non-classical orthogonal polynomials, consider the example of the Bessel polynomials. Inserting $\phi_n(x) = B_n^{(\beta_1, \beta_2)}(x)$ into the right hand side of Eq.(D.7) we obtain,

$$\underbrace{\left[e^{-\frac{\beta_2}{x}} x^{\beta_1+2} \left\{ B_n^{(\beta_1, \beta_2)}(x) \left(\frac{d}{dx} B_m^{(\beta_1, \beta_2)}(x) \right) - \left(\frac{d}{dx} B_n^{(\beta_1, \beta_2)}(x) \right) B_m^{(\beta_1, \beta_2)}(x) \right\} \right]_{x \rightarrow 0}^{x \rightarrow \infty}}_{\text{order } \beta_1 + m + n + 1 \text{ polynomial}}$$

Recall that $\beta_1 < 0$. Again, the polynomial part in the above expression is of order $\beta_1 + m + n + 1$, and hence is completely suppressed by the function $e^{-\frac{\beta_2}{x}}$, in the $x \rightarrow 0$ limit for all m and n . However in the $x \rightarrow \infty$ limit, $e^{-\frac{\beta_2}{x}}$ does not suppress the polynomial expression. Hence in order for the limit to be zero, we require $m + n < -(\beta_1 + 1)$. Performing an equivalent power counting argument for $m = n$, in order to satisfy the following bound on the orthogonality integral,

$$\int_0^\infty dx e^{-\frac{\beta_2}{x}} x^{\beta_1} (B_n^{(\beta_1, \beta_2)}(x))^2 < \infty$$

we obtain the already given restriction of n , $n < -\frac{\beta_1+1}{2}$.

It is an equivalent process to derive the corresponding restrictions associated with the Fisher-Snedecor and Romanovski polynomials. For more information on the classical orthogonal polynomials (Hermite, Laguerre and Jacobi), see Chap. 22 of [16]. For more information on the Bessel polynomials see [17, 25] and references therein. For more information on the Fisher-Snedecor polynomials see [26]. Finally, for more information on the Romanovski polynomials see [18, 27, 28].

Appendix D.9. A word on the Fisher-Snedecor polynomials

The Fisher-Snedecor polynomials are actually the Jacobi polynomials under a scale/translation transformation and greatly increased range. It is this increased range which causes the finite orthogonality property, hence forcing us to place the Fisher-Snedecor polynomials in the *non-classical* category.

Appendix E. Inapplicable parameter cases

Appendix E.1. Laguerre polynomials

For this case we require that $s(x)$ be linear. However, careful inspection of $s(x)$ in Eq. (16) reveals that there is no sensible method to obtain a linear

$s(x)$. Although not applicable in this context, those interested in applying Laguerre polynomials to Fokker-Planck type equations in other contexts are referred to [29] and references therein. One obtains a result similar to the Hermite case, where the infinite bilinear sum of Laguerre polynomials is drastically simplified to a single *modified Bessel function of the first kind* using the *Hille-Hardy* formula.

Appendix E.2. Jacobi and Fisher-Snedecor polynomials

For this case we require that $s(x)$ be quadratic and contain two distinct real roots. However, like the Laguerre case, careful inspection of $s(x)$ reveals that there does not appear to be a sensible way to achieve this. One could attempt to make certain variables complex, but this would have negative consequences on the corresponding Langevin equation. Although not applicable in this context, those interested in applying Jacobi and Fisher-Snedecor polynomials to Fokker-Planck type equations in other contexts are referred to [29] and [30] respectively.

Appendix F. Detailed derivations of spectral cases

We now begin to assign values to the parameters, $\{\gamma_1, \gamma_2, c\}$, in Eq.(C.5). This allows us to generate a specific form for $s(x)$, (constant, linear or quadratic), hence allowing us to pin down the form of the eigenvalues and eigenfunctions of the various cases.

Appendix F.1. Parameter values - Hermite polynomials

For this case we require that $s(x)$ be a constant, hence we assign,

$$\gamma_1 = 0 \text{ and } \{\gamma_2, c\} \in \mathbb{R} \Rightarrow s(x) = \frac{\Omega\gamma_2^2}{2}. \quad (\text{F.1})$$

The corresponding Langevin equation is

$$\dot{x} = \omega - \sigma\lambda x + \gamma_2 c \Gamma_1 + \gamma_2 \sqrt{|1 - c^2|} \Gamma_2.$$

Appendix F.2. The stationary density/weight function

Substituting the above values into Eq.(18) we obtain,

$$\begin{aligned} P_{\text{st}}(x) &= \frac{2}{\Omega\gamma_2^2} \exp \left\{ -\frac{2\sigma\lambda}{\Omega\gamma_2^2} \int dx \left(x - \frac{\omega}{\sigma\lambda} \right) \right\} \\ &= \frac{2}{\Omega\gamma_2^2} \exp \left\{ -\frac{\sigma\lambda}{\Omega\gamma_2^2} \left(x - \frac{\omega}{\sigma\lambda} \right)^2 \right\} \end{aligned} \quad (\text{F.2})$$

where we have assigned the value $\left(\frac{\omega}{\sigma\lambda}\right)^2$ for the integration constant in order to complete the square.

Appendix F.3. Eigenvalue equation

Substituting the parameter values in Eq.(F.1) into Eq.(C.5) and performing the following change in variables,

$$x = \sqrt{\frac{\Omega}{\sigma\lambda}}\gamma_2 z + \frac{\omega}{\sigma\lambda} \quad (\text{F.3})$$

we obtain,

$$\frac{d^2}{dz^2}\varphi_n(z) - 2z\frac{d}{dz}\varphi_n(z) = -\frac{2}{\sigma\lambda}\eta_n\varphi_n(z) = -2n\varphi_n(z). \quad (\text{F.4})$$

The eigenvalue, $\eta_n = \sigma\lambda n$, is obtained from Eq.(D.3). The above equation is known as the *nth order Hermite differential equation* whose solution is the *nth order Hermite polynomial*, $\varphi_n(z) = H_n(z)$, which has the following hypergeometric form,

$$\begin{aligned} H_{2n}(z) &= (-1)^n \frac{(2n)!}{n!} {}_1F_1\left(\begin{matrix} -n \\ \frac{1}{2} \end{matrix} \middle| z^2\right) \\ H_{2n+1}(z) &= (-1)^n \frac{(2n+1)!}{n!} (2z) {}_1F_1\left(\begin{matrix} -n \\ \frac{3}{2} \end{matrix} \middle| z^2\right) \end{aligned}$$

or equivalently from the Rodrigues formula,

$$H_n(z) = (-1)^n e^{z^2} \frac{d^n}{dz^n} e^{-z^2}.$$

Appendix F.4. Analysis at the natural boundaries

Using the details from Appendix C, we have the following form for the potential $V(z)$ in Eq.(C.3),

$$V(z) = \frac{\sigma\lambda}{2} (z^2 - 1) \Rightarrow \lim_{z \rightarrow \pm\infty} V(z) = \infty.$$

Hence we determine that the behaviour of Eq.(F.3) at the boundaries is strictly non-oscillatory, and hence the solution to the probability density is,

$$P(z, z|t, t') = \frac{2}{\Omega\gamma_2^2} e^{-z^2} \sum_{n=0}^{\infty} e^{-\sigma\lambda n(t-t')} \rho_n H_n(z) H_n(z'). \quad (\text{F.5})$$

Appendix F.5. Initial conditions and orthogonality

We now determine the normalisation parameter, ρ_n , through the initial condition,

$$P(z, z'|t, t') = \delta \left(\sqrt{\frac{\Omega}{\sigma\lambda}} \gamma_2(z - z') \right) = \sqrt{\frac{\sigma\lambda}{\Omega}} \frac{1}{|\gamma_2|} \delta(z - z')$$

and applying the Hermite polynomial orthogonality condition,

$$\int_{-\infty}^{\infty} dz e^{-z^2} H_m(z) H_n(z) = \delta_{mn} 2^n n! \sqrt{\pi}. \quad (\text{F.6})$$

We obtain,

$$\rho_n = \sqrt{\frac{\Omega\sigma\lambda}{\pi}} \frac{|\gamma_2|}{2^{n+1}n!}.$$

Thus the probability density is

$$P(z, z'|t, t') = \sqrt{\frac{\sigma\lambda}{\pi\Omega\gamma_2^2}} e^{-z^2} \sum_{n=0}^{\infty} \frac{1}{2^n n!} e^{-\alpha_1 n(t-t')} H_n(z) H_n(z'). \quad (\text{F.7})$$

Appendix F.6. Mehler's formula

Applying *Mehler's formula*,

$$\sum_{n=0}^{\infty} \frac{1}{2^n n!} \xi^n H_n(z) H_n(z') = \frac{1}{\sqrt{1-\xi^2}} \exp \left\{ \frac{2zz' - \xi^2(z^2 + z'^2)}{1-\xi^2} \right\}, \quad -1 < \xi < 1 \quad (\text{F.8})$$

we can eliminate the summation altogether from Eq.(F.7). Expressing the solution in terms of the original x variable the final form of the probability density becomes,

$$\begin{aligned} P(x, x'|t, t') &= \sqrt{\frac{\sigma\lambda}{\pi\gamma_2^2\Omega(1 - e^{-2\sigma\lambda(t-t')})}} \\ &\times \exp \left\{ -\frac{\sigma\lambda}{\gamma_2^2\Omega(1 - e^{-2\sigma\lambda(t-t')})} \left(x - x' e^{-\sigma\lambda(t-t')} - \frac{\omega}{\sigma\lambda} (1 - e^{-\sigma\lambda(t-t')}) \right)^2 \right\} \end{aligned} \quad (\text{F.9})$$

as presented in the main body.

Appendix F.7. Parameter values - Bessel polynomials

For this case we require that $s(x)$ be quadratic and contain one real double root, hence we have the two possibilities,

$$c = 1 \text{ and } \{\gamma_1, \gamma_2\} \in \mathbb{R} \Rightarrow s(x) = \frac{\Omega}{2} (\gamma_1 x - \gamma_2)^2 \quad (\text{F.10})$$

$$\gamma_2 = 0 \text{ and } \{\gamma_1, c\} \in \mathbb{R} \Rightarrow s(x) = \frac{\Omega \gamma_1^2}{2} x^2. \quad (\text{F.11})$$

For this section we shall concentrate on the choice Eq.(F.10), for which the case $c = -1$ can be obtained by reversing the sign of γ_2 . It is an equivalent process to consider the second choice. The corresponding Langevin equation is

$$\dot{x} = \omega - \sigma \lambda x + (\gamma_2 - \gamma_1 y) \Gamma_1.$$

Appendix F.8. The stationary density/weight function

Performing the following change in variables,

$$x = \frac{z}{\gamma_1} + \frac{\gamma_2}{\gamma_1} \quad (\text{F.12})$$

and substituting Eq.(F.10) into Eq.(18) we obtain,

$$P_{\text{st}}(z) = \frac{2}{\Omega z^2} \exp \left\{ \int dz \left(\frac{2}{\Omega \gamma_1} \left(\omega - \frac{\sigma \lambda \gamma_2}{\gamma_1} \right) \frac{1}{z^2} - \frac{2 \sigma \lambda}{\Omega \gamma_1^2} \frac{1}{z} \right) \right\} = \frac{2}{\Omega} z^{\beta_1} e^{-\frac{\beta_2}{z}} \quad (\text{F.13})$$

where,

$$\beta_1 = -\frac{2 \sigma \lambda}{\Omega \gamma_1^2} - 2, \beta_2 = \frac{2}{\Omega \gamma_1} \left(\omega - \frac{\sigma \lambda \gamma_2}{\gamma_1} \right). \quad (\text{F.14})$$

Appendix F.9. Eigenvalue equation - discrete spectrum

Substituting Eqs.(F.10,F.12) into Eq.(C.5) we obtain,

$$z^2 \frac{d^2}{dz^2} \varphi_n(z) + \{(\beta_1 + 2)z + \beta_2\} \frac{d}{dz} \varphi_n(z) = -\frac{2}{\Omega \gamma_1^2} \eta_n \varphi_n(z) = n(n + \beta_1 + 1) \varphi_n(z). \quad (\text{F.15})$$

The eigenvalue, $\eta_n = -\frac{\Omega \gamma_1^2}{2} n(n + \beta_1 + 1)$, is obtained from Eq.(D.3). The above equation is known as the n th order *Bessel differential equation* whose

solution is the n th order Bessel polynomial, $\varphi_n(z) = B_n^{(\beta_1, \beta_2)}(z)$, which has the following hypergeometric form [31],

$$B_n^{(\beta_1, \beta_2)}(z) = {}_2F_0 \left(-n, n + \beta_1 + 1 \middle| -\frac{z}{\beta_2} \right)$$

or equivalently from the Rodrigues formula,

$$B_n^{(\beta_1, \beta_2)}(z) = \frac{1}{\beta_2^n} z^{-\beta_1} e^{\frac{\beta_2}{z}} \frac{d^n}{dz^n} \left(z^{2n+\beta_1} e^{-\frac{\beta_2}{z}} \right).$$

Appendix F.9.1. The highest eigenvalue

We note that the highest eigenvalue, η_N , is bounded by the following real number,

$$\eta_N < \frac{\Omega\gamma_1^2}{2} \times \frac{(\beta_1 + 1)^2}{4} \quad (\text{F.16})$$

as given by Eq.(D.4).

Appendix F.10. Analysis at the natural boundary

Using the details from section Appendix C, we have the following form for the potential $V(z)$ in Eq.(C.3),

$$V(z) = \frac{\Omega\gamma_1^2}{8} \left\{ \frac{z^2(\beta_1 + 1)^2 + 2z\beta_1\beta_2 + \beta_2^2}{z^2} \right\} \Rightarrow \lim_{z \rightarrow \infty} V(z) = \frac{\Omega\gamma_1^2}{8}(\beta_1 + 1)^2$$

$$y(z) = \sqrt{\frac{2}{\Omega\gamma_1^2}} \log_e(x) \Rightarrow \lim_{z \rightarrow \infty} y^2(z)(V(z) - V(\infty)) = 0$$

Hence we determine that the behaviour of Eq.(F.15) at the natural boundary is non-oscillatory for $\eta_n \in \left[0, \frac{\Omega\gamma_1^2}{8}(\beta_1 + 1)^2\right]$ and oscillatory for $\eta_n > \frac{\Omega\gamma_1^2}{8}(\beta_1 + 1)^2$. Hence the explicit form of the probability density is given by,

$$P(z, z'|t, t') = \frac{2}{\Omega} z^{\beta_1} e^{-\frac{\beta_2}{z}} \left\{ \sum_{0 \leq n < -\frac{\beta_1+1}{2}} e^{\frac{\Omega\gamma_1^2}{2}n(n+\beta_1+1)(t-t')} \rho_n B_n^{(\beta_1, \beta_2)}(z) B_n^{(\beta_1, \beta_2)}(z') \right. \\ \left. + \int_0^\infty d\mu e^{-\Lambda(\mu)(t-t')} \rho(\mu) \psi(\mu, z) \psi(\mu, z') \right\}. \quad (\text{F.17})$$

Appendix F.11. Eigenvalue equation - continuous spectrum

Substituting Eqs.(F.10,F.12) into Eq.(C.9) we obtain,

$$z^2 \frac{d^2}{dz^2} \psi(\mu, z) + \{(\beta_1 + 2)z + \beta_2\} \frac{d}{dz} \psi(\mu, z) + \frac{2}{\Omega \gamma_1^2} \Lambda(\mu) \psi(\mu, z) = 0. \quad (\text{F.18})$$

The canonical form of the Bessel equation in [31], (which has poles at $z = \{0, \infty\}$), is given as

$$z^2 \frac{d^2}{dz^2} \psi(\nu, z) + \{2az + b\} \frac{d}{dz} \psi(\nu, z) - (\nu + a)(\nu - a + 1) \psi(\nu, z) = 0$$

with solution, $\psi(\nu, z) = {}_2F_0 \left(a - \nu - 1, a + \nu \mid -\frac{z}{b} \right)$. Comparing this result with Eq.(F.18) we have $2a = \beta_1 + 2$, $b = \beta_2$, and hence,

$$\Lambda(\mu) = -\frac{\Omega \gamma_1^2}{2} \left(\nu + \frac{\beta_1}{2} + 1 \right) \left(\nu - \frac{\beta_1}{2} \right).$$

Knowing that the above eigenvalue is restricted by Eq.(F.16), we let $\nu = i\mu - \frac{1}{2}$, and hence,

$$\begin{aligned} \Lambda(\mu) &= \frac{\Omega \gamma_1^2}{2} \left(\frac{(\beta_1 + 1)^2}{4} + \mu^2 \right), \quad \mu > 0 \\ \Rightarrow \psi(\mu, z) &= {}_2F_0 \left(\frac{\beta_1 + 1}{2} - i\mu, \frac{\beta_1 + 1}{2} + i\mu \mid -\frac{z}{\beta_2} \right) \end{aligned}$$

which is our fundamental solution in the neighbourhood of the finite boundary.

Appendix F.11.1. The Whittaker function

Following Chap.13 of [16], we have the following relation,

$$\psi(\mu, z) = \frac{\Gamma(-2i\mu)}{\Gamma\left(\frac{\beta_1+1}{2} - i\mu\right)} M(\mu, z) + \frac{\Gamma(2i\mu)}{\Gamma\left(\frac{\beta_1+1}{2} + i\mu\right)} M(-\mu, z) \quad (\text{F.19})$$

$$\text{where } M(\pm\mu, z) = \left(\frac{\beta_2}{z} \right)^{\frac{\beta_1+1}{2} \pm i\mu} {}_1F_1 \left(\frac{\beta_1+1}{2} \pm i\mu \mid \frac{\beta_2}{z} \right).$$

The above solution is proportional to the *Whittaker function of the second kind of imaginary order* [32, 33],

$$W_{-\frac{\beta_1}{2}, i\mu} \left(\frac{\beta_2}{z} \right) = e^{-\frac{\beta_2}{2z}} \left(\frac{\beta_2}{z} \right)^{-\frac{\beta_1}{2}} \psi(\mu, z). \quad (\text{F.20})$$

Explicitly the Whittaker functions of the first and second kind, $M_{\kappa,i\mu}(z)$ and $W_{\kappa,i\mu}(z)$ respectively, satisfy the *Whittaker differential equation*,

$$\frac{d^2}{dz^2}W_{\kappa,i\mu}(z) + \left(\frac{\mu^2 + \frac{1}{4}}{z^2} + \frac{\kappa}{z} - \frac{1}{4} \right) W_{\kappa,i\mu}(z) = 0. \quad (\text{F.21})$$

The purpose of establishing this connection between $\psi(z, \mu)$ and $W_{\kappa,i\mu}(z)$ will become clear when we consider the orthogonality conditions of the continuous spectrum eigenfunctions.

Appendix F.12. Initial conditions and orthogonality

We now determine the normalisation factors, ρ_n and $\rho(\mu)$, through the initial condition,

$$P(z, z'|t', t') = \delta\left(\frac{1}{\gamma_1}(z - z')\right) = |\gamma_1|\delta(z - z')$$

and applying the following discrete and continuous orthogonality conditions,

$$\int_0^\infty dz e^{-\frac{\beta_2}{z}} z^{\beta_1} B_m^{(\beta_1, \beta_2)}(z) B_n^{(\beta_1, \beta_2)}(z) = -\delta_{mn} n! \beta_2^{\beta_1+1} \frac{\Gamma(-n - \beta_1)}{2n + \beta_1 + 1} \quad (\text{F.22})$$

$$\int_0^\infty dz e^{-\frac{\beta_2}{z}} z^{\beta_1} \psi(\mu, z) \psi(\nu, z) = \delta(\mu - \nu) \frac{2\pi \beta_2^{\beta_1+1} \Gamma(i\mu) \Gamma(-i\mu)}{\Gamma\left(\frac{\beta_1+1}{2} + i\mu\right) \Gamma\left(\frac{\beta_1+1}{2} - i\mu\right)} \quad (\text{F.23})$$

$$\int_0^\infty dz e^{-\frac{\beta_2}{z}} z^{\beta_1} B_n^{(\beta_1, \beta_2)}(z) \psi(\mu, z) = 0 \quad (\text{F.24})$$

where $0 \leq m, n < -\frac{\beta_1+1}{2}$ for the discrete case(s). Using the above relations, we obtain for ρ_n and $\rho(\mu)$,

$$\begin{aligned} \rho_n &= -\frac{\Omega|\gamma_1|}{2n!} \beta_2^{-\beta_1-1} \frac{2n + \beta_1 + 1}{\Gamma(-n - \beta_1)} \\ \rho(\mu) &= \frac{\Omega|\gamma_1|}{2} \frac{\Gamma\left(\frac{\beta_1+1}{2} + i\mu\right) \Gamma\left(\frac{\beta_1+1}{2} - i\mu\right)}{2\pi \beta_2^{\beta_1+1} \Gamma(i\mu) \Gamma(-i\mu)}. \end{aligned}$$

Hence we obtain the complete form of the probability density for this case, as given in the main body,

$$P(x, x'|t, t') = \frac{|\gamma_1|}{\beta_2^{\beta_1+1}} z^{\beta_1} e^{-\frac{\beta_2}{z}} \left[\sum_{0 \leq n < -\frac{\beta_1+1}{2}} \frac{(-2n - \beta_1 - 1)}{n! \Gamma(-n - \beta_1)} e^{\frac{\Omega\gamma_1^2}{2} n(n+\beta_1+1)(t-t')} \right]$$

$$\begin{aligned}
& \times B_n^{(\beta_1, \beta_2)}(z) B_n^{(\beta_1, \beta_2)}(z') \\
& + \int_0^\infty d\mu \frac{\Gamma\left(\frac{\beta_1+1}{2} + i\mu\right) \Gamma\left(\frac{\beta_1+1}{2} - i\mu\right)}{2\pi\Gamma(i\mu)\Gamma(-i\mu)} e^{-\frac{\Omega\gamma_1^2}{2}\left(\frac{(\beta_1+1)^2}{4} + \mu^2\right)(t-t')} \\
& \times \psi(\mu, z)\psi(\mu, z') \Big]
\end{aligned} \tag{F.25}$$

where $z = \gamma_1 x - \gamma_2$ and $z' = \gamma_1 x' - \gamma_2$.

Appendix F.12.1. A note on the orthogonality relations

The discrete orthogonality relations Eq.(F.22), were given in [17], and the authors noted that the proof requires nothing more than the knowledge of how to apply integration by parts. Our continuous orthogonality relation Eq.(F.23), was adapted from the following relation,

$$\begin{aligned}
\int_0^\infty \frac{dx}{x^2} W_{-\frac{\beta_1}{2}, i\mu}(x) W_{-\frac{\beta_1}{2}, i\nu}(x) &= \delta(\mu - \nu) \frac{2\pi\Gamma(i\mu)\Gamma(-i\mu)}{\Gamma\left(\frac{\beta_1+1}{2} + i\mu\right) \Gamma\left(\frac{\beta_1+1}{2} - i\mu\right)}, \\
&\{\mu, \nu\} > 0
\end{aligned} \tag{F.26}$$

originally given by Wimp [32], which is a particular case of a more general relation involving the Meijer's G -function. The above condition was rederived in [33] by the more elementary means of directly using the properties of the hypergeometric functions ${}_2F_0$ and ${}_1F_1$. We shall adapt the proof in [33] in the next section for the hypergeometric function ${}_2F_1$, thus deriving new orthogonality relations.

Appendix F.13. Parameter values - Romanovski polynomials

For this case we require that $s(x)$ be quadratic and contain two distinct complex roots, hence we assign,

$$c \neq \pm 1 \text{ and } \{\gamma_1, \gamma_2\} \in \mathbb{R} \Rightarrow s(x) = \frac{\Omega}{2} \{(\gamma_1 x - \gamma_2 c)^2 + \gamma_2^2 (|1 - c^2|)\} \tag{F.27}$$

The corresponding Langevin equation is

$$\dot{x} = \omega - \sigma\lambda x + (\gamma_2 c - \gamma_1 x)\Gamma_1 + \gamma_2 \sqrt{|1 - c^2|}\Gamma_2.$$

Appendix F.14. The stationary density/weight function

Performing the change in variables

$$x = \frac{\gamma_2}{\gamma_1} \left(z \sqrt{|1 - c^2|} + c \right) \quad (\text{F.28})$$

and substituting Eq.(F.27) into Eq.(18) we obtain,

$$\begin{aligned} P_{\text{st}}(z) &= \frac{2}{\Omega \gamma_2^2 (|1 - c^2|)(z^2 + 1)} \\ &\times \exp \left\{ \frac{2}{\Omega \gamma_1^2} \int dz \left(\frac{1}{\sqrt{|1 - c^2|}} \left(\frac{\omega \gamma_1}{\gamma_2} - \sigma \lambda c \right) - \sigma \lambda z \right) \frac{1}{z^2 + 1} \right\} \\ &= \frac{2}{\Omega \gamma_2^2 (|1 - c^2|)} (z^2 + 1)^{\beta_1} e^{\beta_2 \arctan(z)} \end{aligned} \quad (\text{F.29})$$

where,

$$\beta_1 = -\frac{\sigma \lambda}{\Omega \gamma_1^2} - 1, \quad \beta_2 = \frac{2}{\Omega \gamma_1^2 \sqrt{|1 - c^2|}} \left(\frac{\omega \gamma_1}{\gamma_2} - \sigma \lambda c \right). \quad (\text{F.30})$$

Appendix F.15. Eigenvalue equation - discrete spectrum

Substituting Eqs.(F.27,F.28) into Eq.(C.5) we obtain,

$$\begin{aligned} \{z^2 + 1\} \frac{d^2}{dz^2} \varphi_n(z) + \{2(\beta_1 + 1)z + \beta_2\} \frac{d}{dz} \varphi_n(z) &= -\frac{2}{\Omega \gamma_1^2} \eta_n \varphi_n(z) \\ &= n(n + 2\beta_1 + 1) \varphi_n(z). \end{aligned} \quad (\text{F.31})$$

The eigenvalue, $\eta_n = -\frac{\Omega \gamma_1^2}{2} n(n + 2\beta_1 + 1)$, is obtained from Eq.(D.3). The above equation is known as the *n*th order *Romanovski differential equation* whose solution is the *n*th order Romanovski polynomial, $\varphi_n(z) = R_n^{(\beta_1, \beta_2)}(z)$. It is possible to transform the *n*th order Romanovski differential equation into the Jacobi differential equation, given as,

$$\begin{aligned} \{1 - \xi^2\} \frac{d^2}{d\xi^2} \varphi_n(\xi) - \{\beta_1 - \beta_2 + (\beta_1 + \beta_2 + 2)\xi\} \frac{d}{d\xi} \varphi_n(\xi) \\ + n(n + \beta_1 + \beta_2 + 1) \varphi_n(\xi) = 0 \end{aligned}$$

where

$$\varphi_n(\xi) = P_n^{(\beta_1, \beta_2)}(\xi) = \frac{(\beta_1 + 1)_n}{n!} {}_2F_1 \left(\begin{matrix} -n & n + \beta_1 + \beta_2 + 1 \\ \beta_1 + 1 \end{matrix} \middle| \frac{1 - \xi}{2} \right). \quad (\text{F.32})$$

Performing the transformation $z = i\xi$ in Eq.(F.31) we obtain,

$$\begin{aligned} \{1 - \xi^2\} \frac{d^2}{d\xi^2} \varphi_n(\xi) - \{-i\beta_2 + 2(\beta_1 + 1)\xi\} \frac{d}{d\xi} \varphi_n(\xi) \\ + n(n + 2\beta_1 + 1) \varphi_n(\xi) = 0. \end{aligned} \quad (\text{F.33})$$

Thus, comparing Eq.(F.33) with Eq.(F.32) we obtain the following hypergeometric form for $R_n^{(\beta_1, \beta_2)}(z)$,

$$R_n^{(\beta_1, \beta_2)}(z) = (2i)^n \left(\beta_1 - i\frac{\beta_2}{2} + 1 \right)_n {}_2F_1 \left(\begin{matrix} -n & n + 2\beta_1 + 1 \\ \beta_1 - \frac{i}{2}\beta_2 + 1 \end{matrix} \middle| \frac{1 + iz}{2} \right).$$

Equivalently, from the Rodrigues formula we obtain,

$$R_n^{(\beta_1, \beta_2)}(z) = (z^2 + 1)^{-\beta_1} e^{-\beta_2 \arctan(z)} \frac{d^n}{dz^n} \left((z^2 + 1)^{n+\beta_1} e^{\beta_2 \arctan(z)} \right).$$

We have not succeeded in progressing the analysis satisfactorily beyond this point.

References

- [1] Y Kuramoto, *Chemical Oscillations, Waves and Turbulence*, Springer, Berlin, (1984)
- [2] S H Strogatz, *From Kuramoto to Crawford: exploring the onset of synchronization in populations of coupled oscillators*, Physica D 143,1 (2000)
- [3] H Sakaguchi, Progr.Theor.Phys. 79, 39 (1988)
- [4] S H Strogatz, R E Mirollo, J.Statist.Phys. 60, 613 (1991)
- [5] J Gomez-Gardenes, Y Moreno, A Arenas, Phys.Rev.E 75, 066106 (2007); Phys.Rev.Lett. 98, 034101 (2007)
- [6] L M Pecora, T L Carroll, Phys.Rev.Lett. 80, 2109 (1998)
- [7] A C Kalloniatis, *From incoherence to synchronicity in the network Kuramoto model*, Phys. Rev. E 82, 066202 (2010)
- [8] S H Park, S Kim, *Noise-induced phase transitions in globally coupled active rotators*, Phys.Rev.E 53, 3425 (1996)

- [9] S Kim, S H Park, C S Ryu, *Noise-enhanced multistability in coupled oscillator systems*, Phys.Rev.Lett. 78, 1616 (1997)
- [10] Z Schuss, *Theory and applications of stochastic processes*, Series in Applied Mathematical Sciences 170, Springer, New York, 2010
- [11] B Bollobás, *Modern Graph Theory* Springer, New York (1998)
- [12] M Fiedler, *Algebraic connectivity of graphs*, Czech. Math. J., 23, 298 (1973)
- [13] A Jadbabaie, N Motee, M Barahona, Proceedings of the American Control Conference, Vol. 5., 4296 (2004)
- [14] P F Gońa, *Stationary Distributions of a Noisy Logistic Process*, Acta Physica Polonica B **36**, No. 6, (2005), 1981-1995
- [15] H Risken, *The Fokker-Planck Equation*, Springer-Verlag, Berlin (1984)
- [16] M Abramowitz and I A Stegun, *Handbook of mathematical functions with formulas, graphs, and mathematical tables*, Dover, New York, (1965)
- [17] H Fakhri and A Chenaghlo, *Ladder operators and recursion relations for the associated Bessel polynomials*, Physics Letters A, **358**, (2006), 345-353
- [18] V Romanovski, *Sur quelques classes nouvelles de polynomes orthogonaux*, C.R. Acad. Sci. Paris, **188**, (1929), 1023-1025
- [19] E Ravasz, A L Barabasi, Phys. Rev. E 67, 026112 (2003)
- [20] A Jamakovic, P van Mieghem, *The Laplacian spectrum of complex networks*, European Conference on Complex Systems, 2006
- [21] H Hong, M Y Choi, B M Kim, *Synchronization on small-world networks*, Phys. Rev. E, **65**, 026139 (2002)
- [22] B Mohar, *The Laplacian spectrum of graphs*, in ‘Graph Theory, Combinatorics, and Applications’, Vol.2. Ed. Y Alavi, G Chartrand, O R Oellerman, A J Schwenk, Wiley, 1991, pp.871-898.

- [23] F R K Chung, *Spectral graph theory*, CBMS Regional Conference Series in Mathematics, No.92, American Mathematical Society, (1996)
- [24] V Linetsky, *The spectral decomposition of the option value*, International Journal of Theoretical and Applied Finance, **7**, No. 3, (2004), 337-384
- [25] H L Krall and O Frink, *A new class of orthogonal polynomials: The Bessel Polynomials*, Trans. Amer. Math. Soc., **65**, (1949), 100-115
- [26] F Avram, N Leonenko and N Šuvak, *On spectral properties and statistical analysis of Fisher-Snedecor diffusion*, <http://arxiv.org/abs/1007.4909>, (2010)
- [27] E J Routh, *On some properties of certain solutions of a differential equation of second order*, Proc. London Math. Soc., **16**, (1884), 245-261
- [28] A P Raposo, H J Weber, D Alvarez-Castillo and M Kirchbach, *Romanovski polynomials in selected physics problems*, Central European Journal of Physics, **5**, Issue 3, (2007), 253-284
- [29] E Wong, *The construction of a class of stationary Markoff processes*, In R. Bellman (ed.), *Stochastic Processes in Mathematical Physics and Engineering*, Providence, RI: American Mathematical Society, (1964), 264-276
- [30] N Leonenko and N Šuvak, *Statistical inference for reciprocal gamma diffusion process*, J. Statist. Plann. Inference, **140**, (2010), 30-51
- [31] P Diță and N Grama, *On Adomian's Decomposition Method for Solving Differential Equations*, <http://arxiv.org/abs/solv-int/9705008>, (1997)
- [32] J Wimp, *A class of integral transforms*, Proc. Edinburgh Math. Soc. 14, (1964), 33-40
- [33] R Szmythkowski and S Bielski, *An orthogonality relation for the Whittaker functions of the second kind of imaginary order*, Integral transforms and special functions, In Press, (2010), <http://arxiv:0910.1492v2>

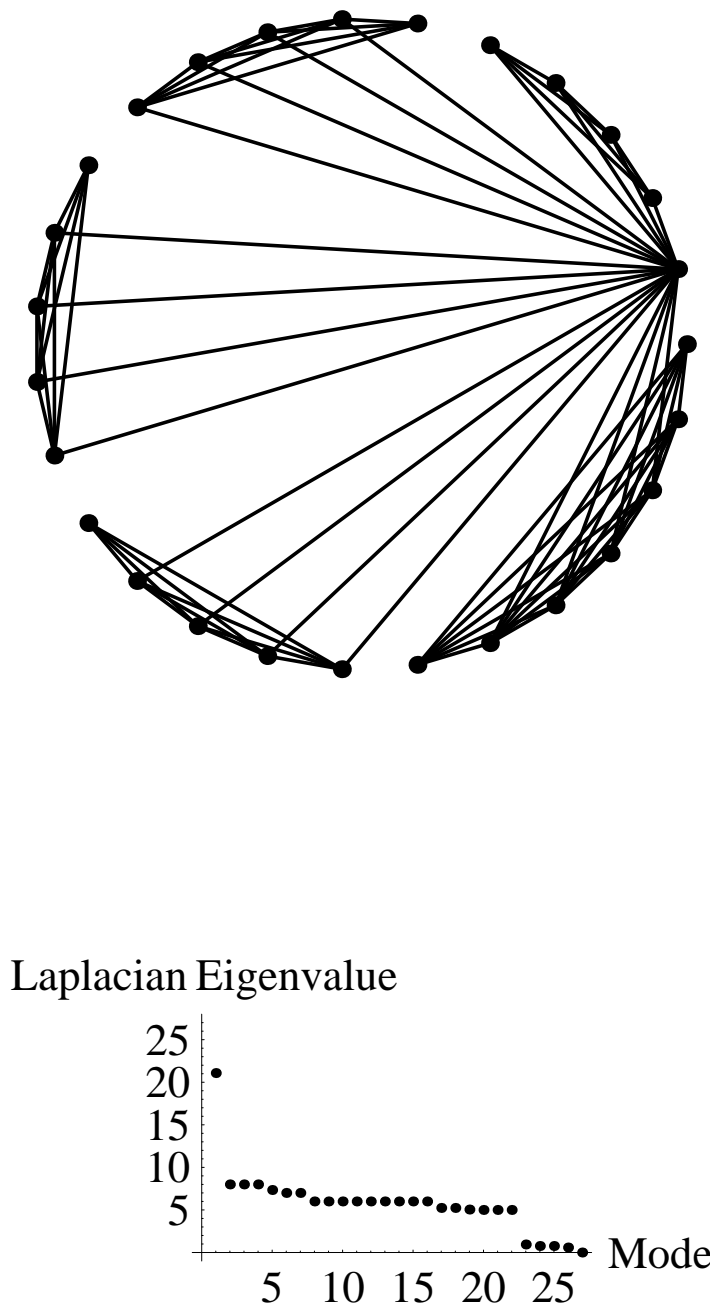


Figure 1: An “RB”-type network represented in a circular embedding shown in the upper panel while its Laplacian spectrum is shown in the lower panel with the eigenvalues plotted in increasing order, from right to left

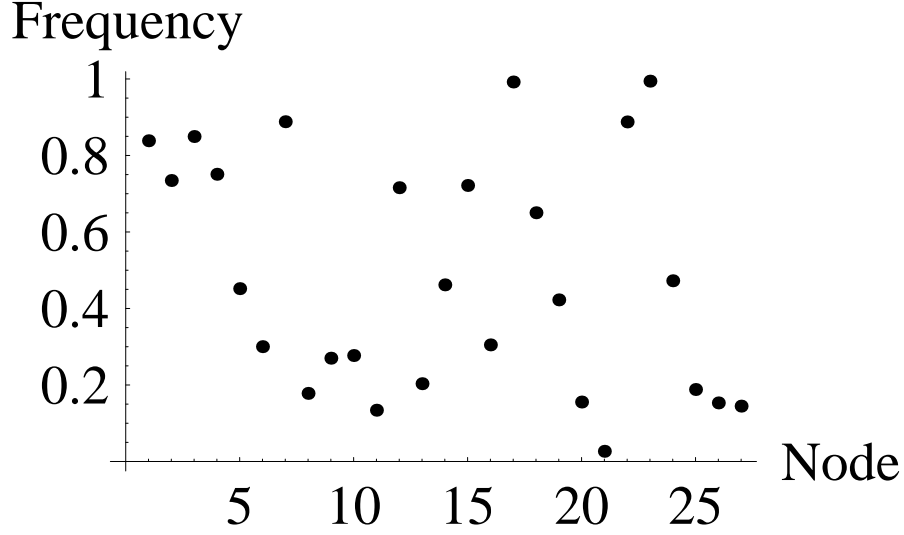


Figure 2: Choice of intrinsic frequencies used in this numerical study which is drawn from a uniform distribution between $[0, 1]$

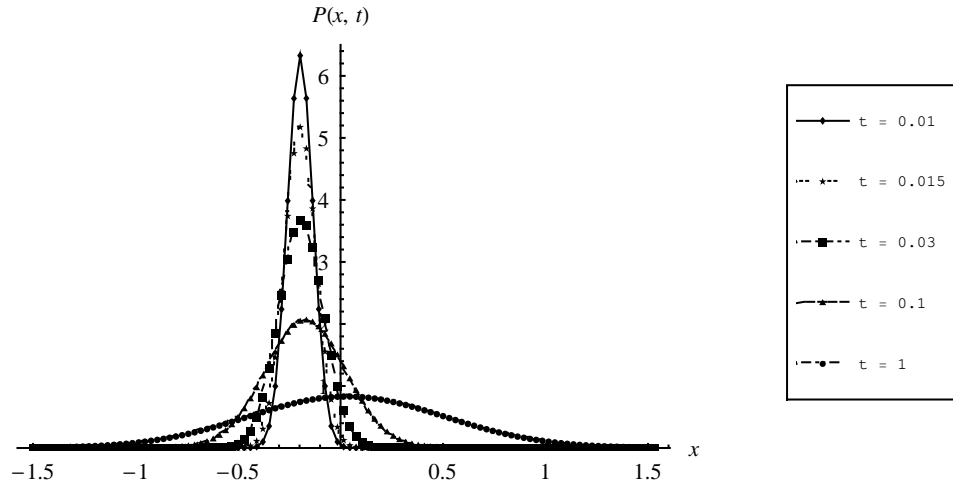


Figure 3: Plot of the probability density, the solution to the Fokker-Planck equation Eq.(17), for different values of time starting from an initial delta function at $x = -0.2$, with noise parameters $\Omega = 0.1$ and $\gamma_1 = 0, \gamma_2 = -2$ which lead to a Hermite decomposition. The series of curves describe the evolution of the $r = 3$ Laplacian eigenmode of the RB graph with $\omega = 0.184, \sigma = 0.8, \lambda = 0.764$.

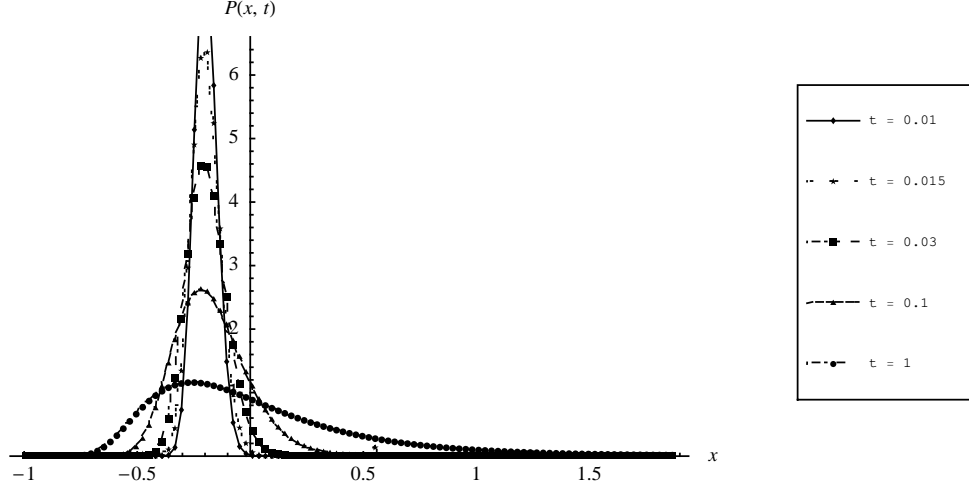


Figure 4: Plot of the probability density, the solution to the Fokker-Planck equation Eq.(17), for different values of time starting from an initial delta function at $x = -0.2$, with noise parameters $\Omega = 0.1$ and $c = 1, \gamma_1 = 2, \gamma_2 = -2$ which lead to a Bessel polynomial decomposition. The series of curves describe the evolution of the $r = 3$ Laplacian eigenmode of the RB graph with $\omega = 0.184, \sigma = 0.8, \lambda = 0.764$.

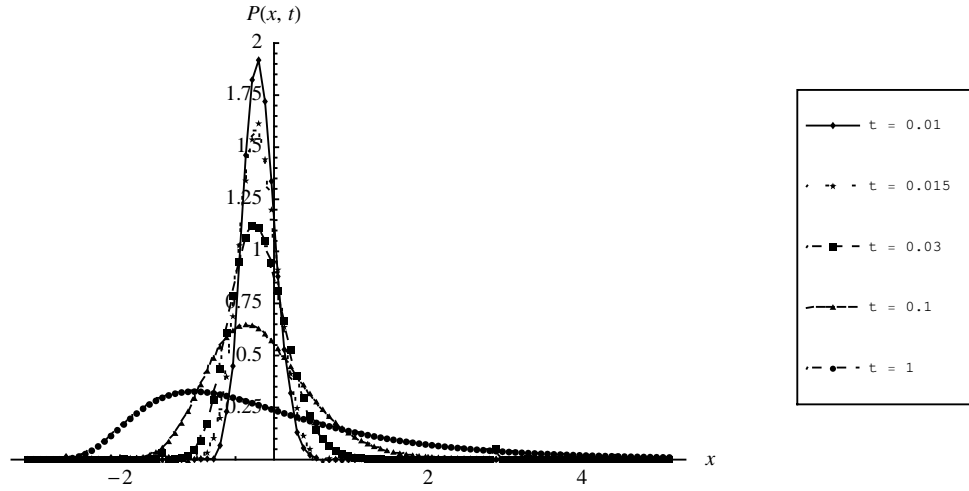


Figure 5: Plot of the probability density, the solution to the Fokker-Planck equation Eq.(17), for different values of time starting from an initial delta function at $x = -0.2$, with noise parameters $\Omega = 0.1$ and $c = 1, \gamma_1 = 2, \gamma_2 = -7$ which lead to a Bessel polynomial decomposition. The series of curves describe the evolution of the $r = 3$ Laplacian eigenmode of the RB graph with $\omega = 0.184, \sigma = 0.8, \lambda = 0.764$.

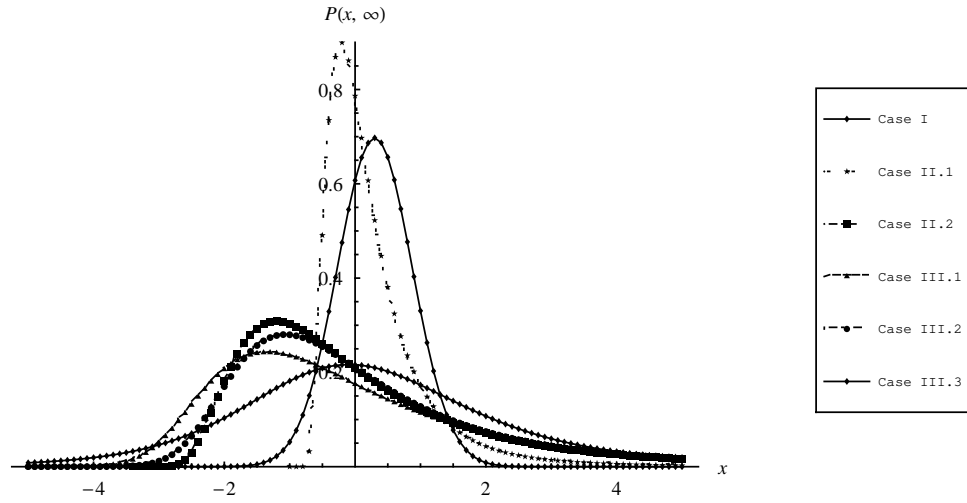


Figure 6: Plots of the stationary probability densities, with noise parameters $\Omega = 0.1$ and various values of c, γ_1, γ_2 . These cases correspond to the $r = 3$ Laplacian eigenmode of the RB graph with $\omega = 0.184, \sigma = 0.8, \lambda = 0.764$.